Rigorous verification of Hopf bifurcations in functional differential equations

Kevin E. M. Church* Jean-Philippe Lessard†

November 4, 2020

Abstract

We propose a rigorously validated numerical method to prove the existence of Hopf bifurcations in functional differential equations of mixed type. The eigenvalue transversality and steady state conditions are verified using the Newton-Kantorovich theorem. The non-resonance condition and simplicity of the critical eigenvalues are verified by either computing a pair of generalized Morse indices of the step map, or by applying the argument principle to the characteristic equation and a suitable contour in the complex plane, computing the contour integral with a rigorous integration approach based on Taylor expansion. As a first application and test problem, we prove the existence of Hopf bifurcations in the Lasota-Wazewska-Czyzewska model and a pair of two such coupled equations. We then use our method to prove the existence of periodic traveling waves in the Fisher equation with nonlocal reaction. These periodic traveling waves are solutions of an ill-posed functional differential equation of mixed type.

1 Introduction

The Hopf bifurcation is a fundamental pathway to oscillations in nonlinear dynamical systems. Since the pioneering work of Henri Poincaré in the late 1800s as applied to ordinary differential equations, this bifurcation has been studied in myriad scenarios, including differential equations in Banach spaces [15, 42], partial differential equations [3, 31, 33, 53, 54], stochastic differential equations [5, 13], functional differential equations [20, 52], and piecewise-smooth systems [26, 55]. Our interest here is in the verification of Hopf bifurcations at equilibrium solutions of functional differential equations, including those of mixed-type. Recall that a functional differential equation of mixed type is an equation of the form

$$\dot{x} = f(x_t),$$

where $f : C([-a, b], \mathbb{R}^n) \to \mathbb{R}^n$ is a functional, $a, b \geq 0$ and $x_t(\theta) \stackrel{\text{def}}{=} x(t+\theta)$ for $\theta \in [-a, b]$. For example, differential difference equations with forward and backward arguments such as

$$\dot{x} = g(x(t), x(t-a), x(t+b))$$

for $g : \mathbb{R}^n \times \mathbb{R}^n \times \mathbb{R}^n \to \mathbb{R}^n$ are of this class. The functional representation for this equation is $f(\phi) \stackrel{\text{def}}{=} g(\phi(0), \phi(-a), \phi(b))$ for $\phi \in C([-a, b], \mathbb{R}^n)$.

Recall the Hopf bifurcation theorem of Rustichini [52] for functional differential equations of mixed-type, which we paraphrase here with a trivial modification concerning the non-stationarity of the equilibrium with respect to parameter variation and the definition of the state space.

*McGill University, Department of Mathematics and Statistics, 805 Sherbrooke Street West, Montreal, QC, H3A 0B9, Canada (kevin.church@mcgill.ca)

†McGill University, Department of Mathematics and Statistics, 805 Sherbrooke Street West, Montreal, QC, H3A 0B9, Canada (jp.lessard@mcgill.ca)

Theorem 1. *Let $\mathcal{I} \subset \mathbb{R}$ be a compact interval containing zero. Suppose $f : C(\mathcal{I}, \mathbb{R}^n) \times \mathbb{R} \to \mathbb{R}^n$ is C^2. Let $\alpha \mapsto x_0(\alpha)$ be a C^2 branch of zeroes of f defined on an open interval containing some $\alpha_0 \in \mathbb{R}$, so that $f(x_0(\alpha), \alpha) = 0$ for $|\alpha - \alpha_0|$ sufficiently small. Let $\sigma(\alpha)$ denote the set of eigenvalues of the linear system*

$$\dot{y} = D_x f(x_0(\alpha), \alpha) y_t.$$

Suppose the following conditions are met.

1. *$\sigma(\alpha_0)$ contains a pair $\pm i\omega_0$ for $\omega_0 > 0$;*
2. *there is a C^1 eigenvalue branch $\lambda(\alpha) \in \sigma(\alpha)$ such that $\lambda(\alpha_0) = i\omega_0$ and $Re(\lambda'(\alpha_0)) \neq 0$;*
3. *$\sigma(\alpha_0) \cap i\mathbb{R} = \pm i\omega_0$ and the pair $\pm i\omega_0$ is simple.*

Then, a Hopf bifurcation occurs at $\alpha = \alpha_0$ in the functional differential equation $\dot{x} = f(x_t, \alpha)$ at the equilibrium $x_0(\alpha_0)$.

Aside from the smoothness requirement, the conditions of the theorem can be summarized as follows. We have (1.) a simple complex-conjugate imaginary pair of eigenvalues that (2.) cross the imaginary axis transversally (3.) without resonance. We briefly recall that the eigenvalues λ of the linearized equation satisfy

$$\Delta(\lambda)v \stackrel{\text{def}}{=} D_x f(x_0(\alpha), \alpha) v \exp_\lambda - \lambda v = 0. \tag{1}$$

where $\exp_\lambda(\theta) \stackrel{\text{def}}{=} e^{\lambda\theta}$. $\Delta(\lambda)$ can be identified with an $n \times n$ matrix, and is called the *characteristic matrix*. The $v \in \mathbb{C}^n$ are the eigenvectors. The domain of $\exp_\lambda$ will depend on the class of problem: namely, it will be the same as the interval $\mathcal{I}$ from the statement of the theorem. For systems of retarded type it will be $\mathcal{I} = [-\tau, 0]$, while for mixed-type equations it can be taken to be $\mathcal{I} = [-a, b]$ for some $\tau > 0$. When $v \in \mathbb{C}^n$, we define $v \exp_\lambda$ to be the function $\theta \mapsto v \exp_\lambda(\theta)$. The eigenvalues also satisfy the *characteristic equation*

$$\det\Delta(\lambda) = 0. \tag{2}$$

This equation is transcendental and has infinitely many solutions, and it is here that the difficulties in rigorous bifurcation verification arise.

Since the eigenvalues of functional differential equations satisfy transcendental equations, it is generally impossible to compute them exactly. In applications, numerical methods are often necessary. There exist several software packages that can test for the existence of bifurcations [1, 18, 57, 19] in delay differential equations, but they are suitable only for non-rigorous numerical exploration. That is, *they can not prove the existence of bifurcations.* In a recent preprint [17], numerical Hopf bifurcation in retarded functional differential equations was studied using a pseudospectral approach. The approach therein is broadly applicable, but verification of non-resonance and simplicity conditions analogous to (3.) from Theorem 1 were unable to be rigorously checked.

While functional differential equations of mixed type frequently come up in the analysis of traveling wave solutions of lattice differential equations [2, 43] and computational approaches have been proposed to solve boundary-value problems and to propagate solutions on half-lines [16, 21, 22, 48, 59], there has been little work done on proving the existence of Hopf bifurcations using the aid of the computer. The Cauchy problem of such equations is generally ill-posed [27], so numerical computation of the eigenvalues based on the characteristic equation seems to be the only available option. While one could envision making use of the holomorphic factorization [44, 45] and the associated semigroups on the "forward" and "backward" space for a functional differential equation of mixed type to compute eigenvalues using a discretization approach, to our knowledge this has not been done.

1.1 Computable conditions for the rigorous verification of Hopf bifurcations

The techniques introduced in the present paper belong to the field of *rigorously validated numerics*. In a broad sense, this field aims at developing numerical methods which can lead to computer-assisted proofs of existence of different type of dynamical objects arising in the study of differential equations. This rather new area of mathematics lies at the intersection of mathematical analysis, scientific computing, approximation theory, topology and numerical analysis. In a nutshell, the goal of rigorously validated numerics is to construct algorithms that provide an approximate solution to a problem together with precise and possibly efficient bounds within which the exact solution is guaranteed to exist in the mathematically rigorous sense. As already mentioned in more details in [7], this requires an a priori setup that allows analysis and numerics to go hand in hand: the choice of function spaces, the choice of the basis functions and Galerkin projections, the analytic estimates, and the computational parameters must all work together to bound the errors due to approximation, rounding, and truncation sufficiently tightly for the verification proof to go through. We encourage the interested reader to consult the books [8, 50, 60] and the survey articles [7, 24, 35, 51] for an introduction to the field.

In this paper, we focus our attention on the rigorous verification of Hopf bifurcations in functional differential equations. While to the best of our knowledge, this has never been achieved before, the rigorous verification of bifurcations in ODEs, PDEs and discrete dynamical systems is not new. Using a Krawczyk-based interval validation method, a computer-assisted approach is proposed in [30] to study turning points, symmetry breaking bifurcation points and hysteresis points in ODEs. Still in the context of finite dimensional dynamical systems, rigorous methods to verify existence of double turning points [47, 58], period doubling bifurcations [61], saddle-node bifurcations [38] and cocoon bifurcations [36] have also been developed. More recently, a method based on desingularization and continuation was proposed in [9] to study Hopf bifurcations in ODEs. Techniques for infinite dimensional dissipative PDEs also started to appear. More explicitly, computational methods for the rigorous verifications of bifurcations of steady states of PDEs are presented in [4, 41, 62] and the recent preprint [10] presents proofs of Hopf bifurcations in the Kuramoto-Sivashinsky equation. An approach to prove rigorously a weaker (topological) notion of bifurcations for steady states of nonlinear partial differential equations is also proposed in [46].

The conditions (1.) and (2.) of Theorem 1, in addition to the branch of steady states, can be made equivalent to the existence of a zero for particular nonlinear map of dimension $6n$. This map is derived in Section 2, and therein we review how the a twist on the standard Newton-Kanrotovich theorem, namely the *radii polynomial method*, can be applied to prove the existence of zeroes.

The non-resonance and simplicity condition (3.) of Theorem 1 is more subtle. We must count the number of eigenvalues on the imaginary axis or, having successfully proven the existence of at least one complex-conjugate pair using the method of Section 2, we must find a neighbourhood of the imaginary axis that contains at most two eigenvalues. To this end, we propose two approaches.

- Use the argument principle to rigorously count the number of zeroes of (1) in a strip containing the imaginary axis.
- Use the Chebyshev spectral method from [39] to compute generalized Morse indices at radii $r = 1 \pm \delta$ for some $\delta > 0$ small, and use these indices to determine an upper bound on the number of zeroes of (2) on the imaginary axis.

The advantage of the first method is that it is general and can be set up for any functional differential equation, including those that involve advanced, delayed or mixed-type arguments, distributed arguments, or combinations thereof. However, a rigorous, general-purpose implementation of this method on the computer would be a difficult programming task. Additionally, we require a priori bounds on the absolute value of the potential Hopf frequencies to select the contour over which to compute. To compare, the Chebyshev spectral method is based on discretizing the step map, and has thus far only been developed rigorously for differential equations with a single discrete delay. However, general-purpose code is available

and no a priori bounds concerning the Hopf frequencies are needed. For systems with a single discrete delay, the code at [12] based on the methods of this paper is general-purpose and can be used to prove the existence of a Hopf bifurcation. Both methods – based on the argument principle and Morse indices – will be discussed in Section 3.

1.2 Example: Hopf bifurcation in the Lasota-Wazewska-Czyzewska model

In [56], Hopf bifurcation in the Lasota-Wazewska-Czyzewska model of red blood cell survival was proven. The rescaled model is given by

$$\dot{x}(t) = -\sigma x(t) + e^{-x(t-\tau)}, \tag{3}$$

for $\sigma > 0$ and $\tau > 0$. Since the equilibria x^* are solutions of the transcendental equation

$$-\sigma x^* + e^{-x^*} = 0,$$

this is a good test problem as the solutions will need to be approximated numerically. Using the methods of this paper, we will prove the following.

Theorem 2. *The Lasota-Wazewska-Czyzewska model has a Hopf bifurcation with respect to the delay τ at the following parameter values and equilibria:*

- $\sigma = 0.3$, $x \in 1.104542018324 + [-1,1]7.2 \times 10^{-13}$, $\tau \in 19.208854104207 + [-1,1]7.2 \times 10^{-13}$.
- $\sigma = 0.35$, $x \in 1.025065556445 + [-1.1]9.8 \times 10^{-13}$, $\tau = 37.030171112739 + [-1,1]9.8 \times 10^{-13}$.

1.3 Application: Coupled Lasota-Wazewska-Czyzewska model

Once again using the techniques of this paper, we will prove some Hopf bifurcations in a system of two coupled Lasota-Wazewska-Czyzewska equations.

Theorem 3. *Consider the coupled Lasota-Wazewska-Czyzewska equations*

$$\begin{aligned}\dot{x}(t) &= -\sigma_1 x(t) + e^{-x(t-\tau)} - \xi x(t) + \rho\xi y(t)\\ \dot{y}(t) &= -\sigma_2 y(t) + e^{-y(t-\tau)} + \xi x(t) - \rho\xi y(t),\end{aligned}$$

where $\xi \geq 0$ is the coupling strength and $\rho \in \{0,1\}$ determines whether coupling is unidirectional ($\rho = 0$) or bidirectional ($\rho = 1$). For $\sigma_1 = 0.1$, $\sigma_2 = 0.5$, and $\tau = 17$, there is a Hopf bifurcation with respect to the parameter ξ at the following parameter values and equilibria:

- $(x,y) \in (1.14466886800860, 1.08412201968491) + [-1,1]^2 \cdot 7.5 \times 10^{-14}$, $\rho = 0$, $\xi \in 0.02809728931663 + [-1,1]7.2 \times 10^{-14}$.
- $(x,y) \in (1.5858236138052, 0.9030535509805) + [-1,1]^2 \cdot 2.1 \times 10^{-13}$, $\rho = 1$, $\xi \in 0.1780972893166 + [-1,1]2.2 \times 10^{-13}$.

1.4 Application: Hopf bifurcation of periodic traveling waves in a nonlocal Fisher equation

It has been suggested [6, 25] that the nonlocal Fisher equation:

$$u_t = Du_{xx} + \mu u(\sigma - \phi * u) \tag{4}$$

might have, for large μ and some diffusion D, wave train (periodic traveling wave) solutions. Wave trains are spatially periodic solutions of the form

$$u(t,x) = \psi(x+ct)$$

for ψ nontrivial and periodic, with c the wave velocity. Here, $\phi \geq 0$ is an integrable function with $\int_{\mathbb{R}} \phi(x)dx = 1$, and $*$ is spatial convolution:

$$(\phi * u)(x) = \int_{-\infty}^{\infty} \phi(y)u(x-y)dy.$$

In [23], numerical results suggested that model (4) with $\phi = \phi_0$,

$$\phi_0(y) = \begin{cases} 1/N, & 0 \leq y \leq N \\ 0 & \text{otherwise} \end{cases}$$

might have stable periodic traveling wave solutions. With the kernel $\phi = \phi_1$,

$$\phi_1(y) = \begin{cases} 1/(2N), & |y| \leq N \\ 0 & \text{otherwise.} \end{cases}$$

pulsating fronts were observed numerically [49]. These are solutions of the form $u(t,x) = \mathcal{U}(x+ct,x)$ for $\mathcal{U}$ periodic in its second variable. Symmetry of the kernel ϕ seems to be a precursor to the existence of pulsating fronts [14], and analytical sufficient conditions for the existence of such fronts have been proven.

Periodic traveling waves of (4) can be identified with periodic solutions of the functional differential equation

$$c\psi'(x) = D\psi''(x) + \mu\psi(x)\left(\sigma - \int_{-\infty}^{\infty} \phi(y)\psi(x-y)dy\right). \tag{5}$$

Depending on the support of the kernel ϕ, this equation can be of retarded, advanced, or mixed-type. We will consider equation (4) with piecewise-constant kernel

$$\phi(y) = \begin{cases} h/N_1 & -N_1 < y < 0 \\ (1-h)/N_2 & 0 < y < N_2 \\ 0 & \text{otherwise.} \end{cases} \tag{6}$$

for $N_1, N_2 > 0$ and $h \in [0,1]$. Equation (5) with the above kernel is of mixed-type whenever $h \notin \{0,1\}$, and in this case the Cauchy problem is ill-posed. Using rigorous verification of Hopf bifurcation, we will prove the following theorem.

Theorem 4. *Consider the nonlocal Fisher equation* (4) *with kernel* ϕ *from* (6) *and* $\sigma = 1$. *Define* $\rho = \mu N_1^2 D^{-1}$. *For periodic traveling waves of the form*

$$u(t,x) = \psi\left(\frac{1}{N_1}x + c\frac{D}{N_1^2}t\right)$$

for ψ *periodic with small amplitude and mean close to* $\sigma = 1$, *we have the following results concerning periodic traveling waves with* critical wave velocities c^**:*

(W1) *For* $N_1 = N_2$, $\rho = 100$ *and* $h = 0.55$, *there exist for* $j = 1,2$, *constants* ξ_j *such that two families of* left-moving *traveling waves exist for* c *such that* $(c - c_j^*)\xi_j > 0$ *for* $|c - c_j^*|$ *sufficiently small. Specifically,* $c_1^* \in -0.499960441060187 + [-1,1]2.6 \times 10^{-15}$ *and* $c_2^* \in -1.407518070559178 + [-1,1]5.7 \times 10^{-15}$.

(W2) *For $N_1 = N_2$, $\rho = 100$ and $h = 0.45$, there exist for $j = 1, 2$, constants ξ_j such that two families of* right-moving *traveling waves exist for c such that $(c - c_j^*)\xi_j > 0$ for $|c - c_j^*|$ sufficiently small. Specifically, $c_1^* \in 0.499960441060186 + [-1, 1]3.3 \times 10^{-15}$ and $c_2^* \in 1.407518070559176 + [-1, 1]7.6 \times 10^{-15}$.*

(W3) *For $N_2/N_1 = 1.05$, $\rho = 100$ and $h = 0.47$, there exist for $j = 1, 2$, constants ξ_j such that two families of traveling waves (one left- and one right-moving) exist for c such that $(c - c_j^*)\xi_j > 0$ for $|c - c_j^*|$ sufficiently small. Specifically, $c_1^* \in -0.363754795740408 + [-1, 1]4.1 \times 10^{-15}$ and $c_2^* \in 0.225343700115205 + [-1, 1]5.9 \times 10^{-15}$.*

(W4) *For $N_1 = 1$, $N_2 = 2$, $\rho = 100$ and $h = 0$, there exist for $j = 1, 2$, constants ξ_j such that two families of* left-moving *traveling waves exist for c such that $(c - c_j^*)\xi_j > 0$ for $|c - c_j^*|$ sufficiently small. Specifically, $c_1^* \in 0.743510960061904 + [-1, 1]2.6 \times 10^{-15}$ and $c_2^* \in 38.377317897727600 + [-1, 1]1.4 \times 10^{-14}$.*

We prove this theorem in Section 4.3. The final configuration coincides with the parameter set from the numerical explorations of Genieys, Volpert and Auger [23], in which stable periodic traveling waves were observed; see Figure 8 from that publication. Since the theorem above is proven by way of Hopf bifurcation from $\psi = 1$ in the traveling wave equation (5), this suggests the numerically observed waves in [23] in fact come from a Hopf bifurcation. In Theorem 4, the constants ξ are related to the direction of the Hopf bifurcation. They can generally be computed from the first Lyapunov coefficient [37] of the dynamics restricted to the centre manifold. We do not perform this computation. We also do not investigate the stability of the traveling wave solutions in the PDE (4) itself, as this is far beyond the scope of our work here.

We observe that with the first two (W1 and W2) conclusions of Theorem 4, the critical wave velocities are seemingly related by velocity reversal: namely, $c_j \mapsto -c_j$. There is a reason for this:

Proposition 5. *Consider the linearization at $v = \sigma$ of the functional differential equation of mixed-type*

$$cv'(x) = v''(x) + \rho v(x)\left(\sigma - h\int_{-1}^{0} v(x-y)dy + (1-h)\int_{0}^{1} v(x-z)dz\right). \tag{7}$$

- *If $h = \frac{1}{2}$, there are imaginary eigenvalues $\lambda = i\omega$, $\omega \neq 0$ if and only if $c = 0$. The frequencies ω satisfy*
$$b(\omega) \stackrel{\text{def}}{=} \omega^2 + \frac{\rho \sin(\omega)}{\omega} = 0.$$
- *If $h \neq \frac{1}{2}$ and $b(\omega) = 0$ for some $\omega \neq 0$, then $\lambda = i\omega$ is an eigenvalue provided the wave velocity c satisfies*
$$c = c^*(h) \stackrel{\text{def}}{=} \frac{\rho(\cos(\omega) - 1)}{\omega^2}(2h - 1).$$

The proof of this proposition is straightforward and is omitted. One can move from (5) to (7) when $N_1 = N_2$ by a simple change of variables. Since the frequencies ω of *some* potential Hopf bifurcations for $h \neq \frac{1}{2}$ are fixed by the equation $b(\omega) = 0$ and the critical wave velocity $c^*(h)$ satifies $c^*(\frac{1}{2}+\epsilon) = -c^*(\frac{1}{2}-\epsilon)$, this explains the velocity reversal observed in the theorem. When $h = \frac{1}{2}$ there are generally two pairs of imaginary eigenvalues, so it is possible a double Hopf bifurcation occurs here. When $N_1 \neq N_2$, there is no simple characterization of the frequencies at the Hopf bifurcation analogous to the above proposition.

Remark 1. *Proposition 5 does not guarantee the existence of a Hopf bifurcation at wave speed $c^*(h)$ when $h \neq \frac{1}{2}$, since that proposition does not rule out the existence of other resonant eigenvalues on the imaginary axis. It merely characterizes those with frequencies ω satisfying $b(\omega) = 0$.*

2 Zero-isolation conditions for Hopf bifurcation and zero-finding problem

Before we begin, it is necessary to introduce some notation. For brevity, let $X = C(\mathcal{I}, \mathbb{R}^n)$. For a functional $f : X \times \mathbb{R} \to \mathbb{R}^n$, we denote $D_1 f$ and $D_2 f$ the partial Fréchet derivatives with respect to the first and second variables, respectively. Mixed and multiple Fréchet derivatives will be denoted by such symbols as $D_2 D_1$ and D_1^2. We also associate to such a functional f a *function*, denoted $f_0 : \mathbb{R}^n \times \mathbb{R} \to \mathbb{R}^n$ and defined by $f_0(x, \alpha) = f(c_x, \alpha)$, where $c_x : \mathcal{I} \to \mathbb{R}^n$ is defined by $c_x(\theta) = x$. The notation for Fréchet derivatives will be the same for f_0.

For a linear map $L : X \to \mathbb{R}^n$, we will sometimes abuse notation and write the action of L on an element $\phi \in X$ by writing $L\phi$ instead as $L\phi(\theta)$. The symbol θ will, from this point on, only ever be used when this abuse of notation is being used. If $B : X \times X \to \mathbb{R}^n$ is a bilinear map, we will write the action on a pair x_1, x_2 using braces: $B[x_1, x_2]$. Finally, if $x \in \mathbb{R}^n$, we will sometimes treat x as an element of X by way of the identification $x \equiv c_x$, with $c_x(s) = x$ for all $s \in \mathcal{I}$. This will usually be in the scope of an evaluation of a linear or bilinear map.

2.1 Steady state, eigenvalue and transversality conditions

The baseline hypothesis of Theorem 1 is that we have a branch of steady states parameterized for α near some α_0. In fact, to have a Hopf bifurcation it is necessary for this branch of steady states to be hyperbolic at α_0, since non-hyperbolicity would cause a violation of the non-resonance condition. We will therefore need to investigate the solvability of the equation

$$f_0(x, \alpha) = 0 \tag{8}$$

for $(x, \alpha) \in \mathbb{R}^n \times \mathbb{R}$. Note the use of the map $f_0 : \mathbb{R}^n \times \mathbb{R} \to \mathbb{R}^n$; this is because a steady state solution is precisely a zero of $f_0(\cdot, \alpha)$. From the implicit function theorem, the existence of a unique curve of zeroes through some (x, α) will depend on whether one can uniquely solve the equation

$$D_1 f_0(x, \alpha)x' + D_2 f_0(x, \alpha) = 0 \tag{9}$$

for $x' \in \mathbb{R}^n$. The equations (8) and (9) will be used to define the steady state portion of our zero-finding problem.

Next, we require $\pm i\omega$ to be a pair of eigenvalues of the linearized equation. From (1), this requires solving the equation

$$D_1 f(x, \alpha)v \exp_{i\omega} -i\omega v = 0. \tag{10}$$

The eigenvector v corresponding to this imaginary eigenvalue will also need to be computed. However, since we will ultimately want to identify Hopf bifurcations by computing and verifying data including the eigenvector v, the lack of uniqueness of the eigenvector is a problem. To circumvent this issue, we *assume* we have already computed a numerical candidate eigenvector $\overline{v}$, fix an integer $m \in \{1, \ldots, n\}$, and introduce a function $h_m : \mathbb{C}^{n-1} \to \mathbb{C}^n$ defined by

$$h_m(z) = \begin{bmatrix} z_1 & \cdots & z_{m-1} & \overline{v}_m & z_m & \cdots & z_{n-1} \end{bmatrix}^\intercal. \tag{11}$$

We then replace equation (10) with

$$D_1 f(x, \alpha) \exp_{i\omega} h_m(v) - i\omega h_m(v) = 0. \tag{12}$$

A solution (ω, v) of (10) then uniquely defines a complex eigenvalue-eigenvector pair $(i\omega, h_m(v))$. Related to this equation is

$$D_1 f(x, \alpha)h_m(v) \exp_\lambda -\lambda h_m(v) = 0, \tag{13}$$

which is merely what we would get had we not assumed an imaginary eigenvalue but still fixed the mth component of the eigenvector using the h_m function.

Finally, we need to deal with the eigenvalue transversality condition. We will implicitly differentiate (13) with respect to α. To accomplish this, first recall by the Riesz representation theorem that a functional $L : X \to \mathbb{R}^n$ can be represented in the form

$$L\phi = \int_{\mathcal{I}} [dK(s)]\phi(s)$$

for $K(s)$ matrix-valued and of bounded variation. Then,

$$L\frac{d}{d\alpha}\exp_{\lambda(\alpha)} = \int_I [dK(s)]\frac{d}{d\alpha}e^{\lambda(\alpha)\theta} = \int_I [dK(s)]e^{\lambda(\alpha)\theta}\lambda'(\alpha)\theta = \lambda'(\alpha)L\theta e^{\lambda(\alpha)\theta}.$$

Making use of this calculation and the chain rule, we complete the implicit differentiation of (13) and ultimately evaluate at $\lambda = i\omega$, obtaining

$$\begin{aligned} 0 &= D_1^2 f(x,\alpha)[x', h_m(v)\exp_{i\omega}] + D_2 D_1 f(x,\alpha)h_m(v)\exp_{i\omega} + \lambda'(D_1 f(x,\alpha)\theta e^{i\omega\theta} - I)h_m(v) \\ &\quad + D_1 f(x,\alpha)j_m(v')\exp_{i\omega} - i\omega j_m(v') \\ &\equiv F_4(x, x', \alpha, \omega, v, \lambda', v'), \end{aligned} \tag{14}$$

where j_m is defined by

$$j_m(z) = \left[\begin{array}{ccccccc} z_1 & \cdots & z_{m-1} & 0 & z_m & \cdots & z_{n-1} \end{array}\right]^{\mathsf{T}}. \tag{15}$$

Here, we interpret $v' \in \mathbb{C}^{n-1}$ as the derivative of $v \in \mathbb{C}^{n-1}$ at the parameter value α for which $\lambda = i\omega$. We can then prove the following.

Theorem 6 (Zero-isolation condition for Hopf bifurcation)**.** *Fix some $m \in \{1, \ldots, n\}$ and $\overline{v}_m \in \mathbb{C}$. Let $u_0 = (x_0, x_0', \alpha_0, \omega_0, v_0, \lambda_0', v_0') \in \mathbb{R}^n \times \mathbb{R}^n \times \mathbb{R} \times \mathbb{R} \times \mathbb{C}^{n-1} \times \mathbb{C} \times \mathbb{C}^{n-1}$ be an* isolated *zero of the nonlinear map F defined as follows:*

$$(x, x', \alpha, \omega, v, \lambda', v') \mapsto F(u) = \left[\begin{array}{c} f_0(x,\alpha) \\ D_1 f_0(x,\alpha)x' + D_2 f_0(x,\alpha) \\ D_1 f(x,\alpha)h_m(v)\exp_{i\omega} - i\omega h_m(v) \\ F_4(x, x', \alpha, \omega, v, \lambda', v') \end{array}\right] = \left[\begin{array}{c} F_1(x,\alpha) \\ F_2(x, x', \alpha) \\ F_3(x, \alpha, \omega, v) \\ F_4(x, x', \alpha, \omega, v, \lambda', v') \end{array}\right].$$

There exists a unique C^2 curve $x_0 : (\alpha_0 - \epsilon, \alpha_0 + \epsilon) \to \mathbb{R}^n$ for some $\epsilon > 0$ such that $x_0(\alpha_0) = x_0$. Furthermore, the conditions (1.) and (2.) of Theorem 1 are satisfied provided v_0 and $\overline{v}_m$ are not both zero, and $Re(\lambda_0') \neq 0$.

Proof. Since the zero u_0 is isolated, the kernel of $D_1 f_0(x_0, \alpha_0)$ must be trivial, from which the implicit function theorem guarantees the existence of the unique steady state curve. The existence of the imaginary eigenvalues $\pm i\omega$ follows from the equation $D_1 f(x_0, \alpha_0)h_m(v)\exp_{i\omega} - i\omega h_m(v) = 0$, the assumption on v_0 and $\overline{v}_m$ which guarantees $h_m(v_0) \neq 0$, and the complex-conjugate parity of eigenvalues for real systems. The existence of the C^1 eigenvalue branch $\alpha \mapsto \lambda(\alpha)$ in $\sigma(\alpha)$ with $\lambda(\alpha_0) = i\omega_0$ follows once again from the implicit function theorem and the isolation of u_0, this time applied to $F_4(u_0) = 0$. We get transversality from the assumption $\mathrm{Re}(\lambda_0') \neq 0$ and the equality $\lambda_0' = \frac{d}{d\alpha}\lambda(\alpha_0)$. □

2.2 Verifying zeroes of F using the radii polynomial approach

The nonlinear map F defined in Theorem 6 can be more formally described as $F : U \to V$, where

$$\begin{aligned} U &= \mathbb{R}^n \times \mathbb{R}^n \times \mathbb{R} \times \mathbb{R} \times \mathbb{C}^{n-1} \times \mathbb{C} \times \mathbb{C}^{n-1}, \\ V &= \mathbb{R}^n \times \mathbb{R}^n \times \mathbb{C}^n \times \mathbb{C}^n. \end{aligned}$$

Remark that as real vector space, U and V are $6n$-dimensional. If an approximate zero u_0 of F has been computed, we can verify the existence of a nearby isolated zero using the radii polynomial approach.

Theorem 7. *Let $F : U \to V$ be continuously differentiable and U, V be finite-dimensional vector spaces. Let $u_0 \in U$ be given, and suppose there exists $A : V \to U$ injective and constants $Y_0 \geq 0$, $Z_0 \geq 0$ and $Z_2 : [0, \infty) \to [0, \infty)$ such that*

$$\begin{aligned} ||AF(u_0)||_U &\leq Y_0 \\ ||I_U - ADF(u_0)||_{B(U)} &\leq Z_0 \\ \sup_{\delta \in \overline{B_r(0)}} ||A[DF(u_0+\delta) - DF(u_0)]||_{B(U)} &\leq Z_2(r). \end{aligned}$$

where $||\cdot||_U$ is a norm on U and $||\cdot||_{B(U)}$ is the induced operator norm. Define the radii polynomial

$$p(r) = (Z_2(r) + Z_0 - 1)r + Y_0.$$

If there exists $r_0 > 0$ such that $p(r_0) < 0$, then F has a unique zero in the ball $B_{r_0}(u_0)$.

In practice, A will be a machine computed inverse of $DF(u_0)$ and we will use of Taylor's theorem to determine the $Z_2(r)$ bound. More precisely, for any $\delta \in B_r(0)$ and integer order $k \geq 0$, we have the following bound due to the Lagrange remainder:

$$||A[DF(u_0+\delta) - DF(u_0)]||_{B(U)} \leq \left|\left|\sum_{j=1}^{k} \frac{1}{j!} AD^{j+1}F(u_0)\delta^j\right|\right|_{B(U)} + \frac{1}{(k+1)!}||AD^{k+2}F(u_0+s\delta)\delta^k||_{B(U)}$$

for some $s \in [0,1]$. If $k = 0$, the sum is treated as an empty sum and vanishes. Here, where $\delta^j \overset{\text{def}}{=} [\delta, \ldots, \delta, \cdot]$ with j copies of δ. Formally, $\delta^j : U \to U^{j+1}$ is a nonlinear map that sends $u \in U$ to $[\delta, \ldots, \delta, u] \in U^{j+1}$. In this way, since $D^{j+1}F(u_0) : U^{j+1} \to V$ is $(j+1)$-linear, each of $AD^{j+1}F(u_0)\delta^j$ is a linear operator on U defined by

$$u \mapsto AD^{j+1}F(u_0)\delta^j u = AD^{j+1}f(u_0)[\delta, \ldots, \delta, u].$$

It follows that we can take

$$Z_2(r) = \sup_{\delta \in \overline{B_r(0)}} \left|\left|\sum_{j=1}^{k} \frac{1}{j!} AD^{j+1}F(u_0)\delta^j\right|\right|_{B(U)} + \sup_{s\in[0,1]} \sup_{\xi \in \overline{B}_r(0)} \frac{1}{(k+1)!}||AD^{k+2}F(u_0+s\xi)\xi^k||_{B(U)} \quad (16)$$

as the Z_2 bound. It is straightforward to get an upper bound for this quantity using interval arithmetic once the Fréchet derivatives have been computed.

2.3 Implementation for the case of a single discrete delay

Here we will assume the functional f only has a single discrete delay. That is, we restrict to delay differential equations of the form

$$x'(t) = f(x(t), x(t-\tau), \alpha), \quad (17)$$

where now, $f : \mathbb{R}^n \times \mathbb{R}^n \times \mathbb{R} \to \mathbb{R}^n$ is assumed C^∞ in a neighbourhood of (x_0, x_0, α_0) for the candidate zero u_0 of F, and expressible in terms of elementary functions. We can formally identify the functional that defines the right-hand side of (17). It is

$$C([-\tau, 0], \mathbb{R}^n) \times \mathbb{R} \ni (\phi, \alpha) \mapsto f(\phi(0), \phi(-\tau), \alpha) \equiv \tilde{f}(\phi, \alpha).$$

We want to express the nonlinear map F from Theorem 6 in terms of the discrete-delay functional $\tilde{f}$. It suffices to write down the components F_1 through F_4. The first one is obvious:

$$F_1(x,\alpha) = f(x,x,\alpha). \tag{18}$$

Let D_j denote the partial Fréchet derivative with respect to the jth variable. Then F_2 is

$$F_2(x,x',\alpha) = (D_1 f(x,x,\alpha) + D_2 f(x,x,\alpha))x' + D_3 f(x,x,\alpha). \tag{19}$$

To compute F_3, we will need a representation for the Fréchet derivative $D_1\tilde{f}(x,\alpha)$. From its definition, we have for $\phi \in C([-\tau,0],\mathbb{R}^n)$,

$$D_1\tilde{f}(x,\alpha)\phi = D_1 f(x,x,\alpha)\phi(0) + D_2 f(x,x,\alpha)\phi(-\tau).$$

This together with linearity of $D_2 f(x,x,\alpha)$ implies the representation

$$F_3(x,\alpha,\omega,v) = (D_1 f(x,x,\alpha) + e^{-i\omega\tau}D_2 f(x,x,\alpha) - i\omega I)h_m(v). \tag{20}$$

To compute F_4, we need expressions for $D_1^2\tilde{f}$ and $D_2D_1\tilde{f}$. For $\phi,\psi \in C([-\tau,0],\mathbb{R}^n)$,

$$\begin{aligned} D_2D_1\tilde{f}(x,\alpha)\phi &= D_3D_1 f(x,x,\alpha)\phi(0) + D_3D_2 f(x,x,\alpha)\phi(-\tau), \\ D_1^2\tilde{f}(x,\alpha)[\phi,\psi] &= D_1^2 f(x,x,\alpha)[\phi(0),\psi(0)] + D_2D_1 f(x,x,\alpha)[\phi(0),\psi(-\tau)] \\ &\quad + D_1D_2 f(x,x,\alpha)[\phi(-\tau),\psi(0)] + D_2^2 f(x,x,\alpha)[\psi(-\tau),\psi(-\tau)]. \end{aligned}$$

Using these in (14) and simplifying with bilinearity, we get, for $u = (x,x',\alpha,\omega,v,\lambda',v')$ as in Theorem 6,

$$\begin{aligned} F_4(u) &= D_1^2 f(x,x,\alpha)[x',h_m(v)] + e^{-i\omega\tau}D_2D_1 f(x,x,\alpha)[x',h_m(v)] + D_1D_2 f(x,x,\alpha)[x',h_m(v)] \\ &\quad + e^{-i\omega\tau}D_2^2 f(x,x,\alpha)[x',h_m(v)] + D_3D_1 f(x,x,\alpha)h_m(v) + e^{-i\omega\tau}D_3D_2 f(x,x,\alpha)h_m(v) \\ &\quad - \lambda'(\tau e^{-i\omega\tau}D_2 f(x,x,\alpha) + I)h_m(v) + (D_1 f(x,x,\alpha) + e^{-i\omega\tau}D_2 f(x,x,\alpha) - i\omega I)j_m(v'). \end{aligned} \tag{21}$$

To build the radii polynomial, we first require several partial derivatives of $F = (F_1,F_2,F_3,F_4)$ from (18)–(21). Rather than explicitly write down the various partial derivatives (of which there are many), we rely instead on MATLAB's symbolic algebra toolbox. First, we use the toolbox to build a realified version of the map $F : U \to V$, which we also denote $F : \mathbb{R}^{6n} \to \mathbb{R}^{6n}$, based on a user-inputted anonymous function of the form

`@(x,xtau,alpha,para)f(x,xtau,a,para)`.

The interpretation of `x` and `xtau` are $x(t)$ and $x(t-\tau)$. The variable `a` is the bifurcation parameter α, and `para` is a vector of any other possible parameters or numerical constants that appear in the vector field. This is done so that any of these numerical constants can be properly passed as intervals later when we want to validate a zero of F with interval arithmetic and the radii polynomial. Additional documentation appears in the function files at [12].

The resulting symbolic function version of F is saved, and a multivariable Taylor expansion of this symbolic function is computed to a prescribed order k using the `taylor` function. The expansion is symbolically scaled by $k!$ before being converted to a MATLAB function file. This step is a cheap trick to prevent MATLAB from saving a function file that contains string expressions of doubles that can not be represented as a 64-bit double precision floating point numbers due to the Taylor expansion having terms of the form $1/j!$ for $j = 1,\ldots,k$. The coefficients of the re-scaled Taylor expansion will be representable as 64-bit doubles so long as the order k satisfies $k! \leq 2^{53}$, so practically speaking this is not a limitation.

Once these function files are saved, the radii polynomial is constructed. We undo the scaling by $k!$ using interval arithmetic. We get the Z_2 bound using the Taylor expansion with Lagrange remainder

from (16). The system constants `para` and the delay `tau` are passed as machine precision thin intervals. The result is an interval representation of the radii polynomial. By choosing an a-priori maximum radius r^*, we can take the bound $Z_2(r) \leq Z_2(r^*)$ and compute the zero r_0 of

$$p^*(r) = (Z_2(r^*) + Z_0 - 1)r + Y_0.$$

If $r_0 < r^*$, we then explicitly check that $p(r_0) < 0$ using interval arithmetic. The result is that given an approximate zero u_0 of F, the zero-isolation conditions of Theorem 6 are automatically checked for the true zero $u \in B_{u_0}(r_0)$. This makes up a large part of the Hopf bifurcation conditions for systems of delay differential equations. The condition at the end of the theorem concerning the eigenvector being nonzero can be accomplished by explicitly requiring $\overline{v}_m \neq 0$ to machine precision. As for $\mathrm{Re}(\lambda') \neq 0$, it is enough to find a radius r_0 such that the radii polynomial satisfies $p(r_0) < 0$ and $0 \notin \mathrm{Re}(\lambda_0') + r_0[-1, 1]$. The MATLAB function `prove_Hopf_isolation.m` is a complete implementation of this proof process.

3 Verification of non-resonance and simplicity

Here we outline two approaches to verify the non-resonance condition and the simplicity of the imaginary eigenpair $i\omega_0$ that is required for condition (3.) of Theorem 1. The first is based on computation of generalized Morse indices for the step map, and is applicable to equations with delayed arguments. The second one is based on contour integration and the argument principle, and can be applied to general functional differential equations.

3.1 Difference of generalized Morse indices and step map for delay equations

For discrete delay equations, we use a Chebyshev spectral method for the discretization of the step map [39]. Using this method, one can rigorously prove (under certain conditions) that the step map and its discretization have the same number of eigenvalues of the step map outside of a given closed ball of radius r centered at zero. This number of eigenvalues outside a given ball of radius r is called the *generalized Morse index* and it is denoted μ_r. If this number of eigenvalues is proven to be equal for both the discretization and the full, infinite-dimensional operator, we will say μ_r has been validated. Since an imaginary eigenvalue $\lambda = e^{i\omega}$ corresponds to an eigenvalue of the step map on the unit circle, we can obtain an *upper bound* for the number of imaginary eigenvalues by computing the difference $\mu_{1-\delta_1} - \mu_{1+\delta_2}$ for two positive offsets $\delta_1, \delta_2 > 0$.

To accomplish the proof, there are three technical bounds denoted C_1, C_2 and C_3 that must be computed [39] with interval arithmetic. If their product $C \stackrel{\text{def}}{=} C_1C_2C_3$ satisfies $C < 1$, then μ_r is theoretically validated. The final step that needs to be done is to rigorously compute the eigenvalues of the discretization of the step map. This can be done with `verifyeig` of INTLAB or with the radii polynomial approach [11].

Assume we have a delay differential equation

$$\dot{x} = f(x(t), x(t-\tau), \alpha)$$

depending on the parameter α, we have located a candidate isolated zero u_0 of the map F from Theorem 6, and that the radii polynomial as implemented in Section 2.3 is negative at some $r_0 > 0$. We compute the linearization

$$\dot{y} = D_1 f(x_0, x_0, \alpha_0)y(t) + D_2 f(x_0, x_0, \alpha_0)y(t-\tau),$$

and replace each of x_0 and α_0 with intervals $[x_0 - r_0, x_0 + r_0]$ and $[\alpha_0 - r_0, \alpha_0 + r_0]$. We then choose some $\delta_1, \delta_2 > 0$ and rigorously compute the difference of Morse indices $D(\delta_1, \delta_2) \stackrel{\text{def}}{=} \mu_{1-\delta_1} - \mu_{1+\delta_2}$. We simply compute each one rigorously and take the difference. If $D(\delta_1, \delta_2) = 2$, then we have proven the simplicity and non-resonance conditions for the Hopf bifurcation. Indeed, we already know that $i[\omega_0 - r_0, \omega_0 + r_0]$

contains an imaginary eigenvalue and this interval does not intersect zero, so its complex conjugate defines precisely the second eigenvalue in the count $D(\delta_1, \delta_2) = 2$. This proves the non-resonance, and since the indices count multiplicities, we can conclude that the eigenvalues $\pm i\omega_0$ are simple.

The function `prove_non_resonance.m` completes this calculation. It takes as its inputs the matrices $K_1 = D_1 f(x_0, x_0, \alpha_0)$, $K_2 = D_2 f(x_0, x_0, \alpha_0)$, the delay τ, the dimension n of the system, a number N of modes to use in the Chebyshev spectral method, a weight $\nu > 1$ in the sequence space (see [39] for details), the offsets δ_1 and δ_2, as well as some data relating to the mesh needed to verify the Morse indices (m, the number of mesh points, a flag for uniform or adaptive step size, and a parameter that specifies if the eigenvalues of interval matrices should be validated by the radii polynomial approach [11] or using `verifyeig`). The function `F_Hopf_build.m` that is called during a run of `prove_Hopf_isolation.m` will output functions `Jacobian_0.mat` and `Jacobian_tau.mat` that can be respectively used to compute K_1 and K_2.

3.2 Rigorous contour integration and the argument principle

If we have proven the existence of a candidate Hopf bifurcation for which conditions (1.) and (2.) of Theorem 1 have been verified, we are left with proving that the characteristic equation (2) has at most two zeroes on the imaginary axis (or at most one with positive imaginary part). In what follows, we will assume that we are able to prove an a priori upper bound $\hat{\omega}$ such that any imaginary eigenvalue $\lambda = i\omega$ must satisfy $|\omega| \leq \hat{\omega}$. We will perform the change of variables $z = e^{\lambda}$ to map zeroes of (2) onto the unit circle. This is not strictly necessary, but to make the comparison with the approach based on generalized Morse indices it is helpful. Recalling the characteristic matrix $\Delta(\lambda)$ defined in (1), it suffices to compute the number of zeroes of the nonlinear function

$$g(z) \stackrel{\text{def}}{=} \det \Delta(\log(z))$$

contained in some rectangle of the form

$$(r, \theta) \in [1 - \delta, 1 + \delta] \times [-\epsilon, \hat{\omega} + \epsilon]$$

in polar coordinates, where $\delta > 0$ is chosen small enough so that any other zeroes of g that are *not* on the unit circle are excluded from the rectangle, and $0 < \epsilon \ll |\omega_0|$. In the above, log is understood to be a smooth branch relative to the Riemann surface defined by the polar coordinates rectangle on which we must count zeroes. Denote by $\Gamma = \Gamma_{\delta,\epsilon,\hat{\omega}}$ the positively oriented simple closed curve in $\mathbb{C}$ consisting of the boundary of the above rectangle (see Figure 1 for an example). As long as f is continuously differentiable, the characteristic matrix is continuous in its argument and g will have no poles inside Γ provided $\delta < 1$. If f is analytic, g is meromorphic – in fact, analytic – in Γ. Since any strip in $\mathbb{C}$ contains finitely-many eigenvalues – see Lemma 4.3 from [29] – the number of zeroes of g inside of Γ is finite.

By Cauchy's argument principle

$$N_{\text{zeros}} - N_{\text{poles}} = \frac{1}{2\pi i} \oint_{\Gamma} \frac{g'(z)}{g(z)}\, dz,$$

where N_{zeros} and N_{poles} denote respectively the number of zeros and poles of $g(z)$ inside the contour Γ. Since the function g does not have any poles inside Γ, then the number of zeros inside Γ is simply given by the formula

$$N_{\text{zeros}} = \frac{1}{2\pi i} \oint_{\Gamma} \frac{g'(z)}{g(z)}\, dz.$$

By decomposing the contour Γ as a finite union of shorter contours, $\Gamma = \bigcup_{k=1}^{m} \gamma_k$,

$$N_{\text{zeros}} = \frac{1}{2\pi i} \sum_{k=1}^{m} \int_{\gamma_k} \frac{g'(z)}{g(z)}\, dz. \tag{22}$$

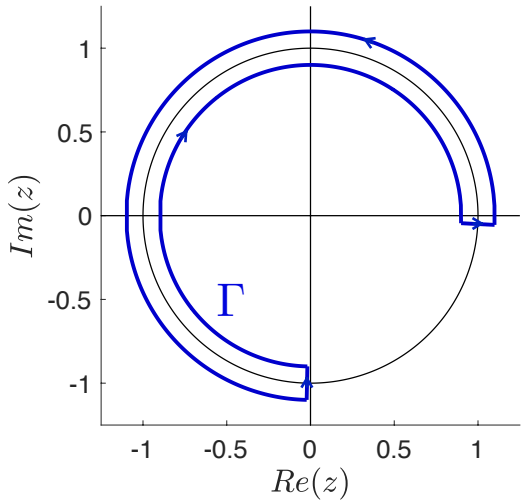

Figure 1: Example of a contour Γ.

The rest of this section is therefore dedicated to implement a validated numerical scheme for evaluating the contour integrals on the right hand side of (22), hence obtaining the desired count of zeros of g.

Considering a short contour γ tracing a curve from the point $z_0 \in \mathbb{C}$ to another point $z_1 \in \mathbb{C}$. The idea of the approach is to transform the computation of

$$\int_\gamma \frac{g'(z)}{g(z)} dz \tag{23}$$

into one of computing the solution of an initial value problem of a polynomial complex valued vector field. This approach falls into the more general method of automatic differentiation or *polynomial embedding* (e.g. see [28, 32, 40]). Recall that if f is polynomial, then $g(z) = \det \Delta(\log(z))$ involves a combination of powers of $\log(z)$ and z^α, for different values of $\alpha \in \mathbb{R}$. If f is not polynomial but involves combination of analytic functions which are themselves solutions of polynomial ODEs, then the polynomial embedding approach is still applicable. It goes as follows. Define intermediate variables $u_1(z) \stackrel{\text{def}}{=} 1/z$, $u_2(z) \stackrel{\text{def}}{=} \log(z)$, $u_3(z) \stackrel{\text{def}}{=} z^\alpha, \ldots, u_{p-3}(z)$ in a way that one can write, for each $k = 1, \ldots, p-3$, a complex valued ODE of the form $u_k' = \Phi_k(u_1, \ldots, u_{p-3})$, where Φ_k is a polynomial in $u_1, \ldots, u_{p-3}$. For instance, $u_1'(z) = -1/z^2 = -u_1^2$, $u_2'(z) = 1/z = u_1$ and $u_3'(z) = \alpha z^\alpha / z = \alpha u_1 u_3$ are all polynomial ODEs in the variables u_1, u_2, u_3. Let $u_{p-2}(z) \stackrel{\text{def}}{=} g'(z)$. Since g involves a combination of powers of $\log(z)$ and z^α, $u_{p-2}'(z) = \Phi_{p-2}(u_1, \ldots, u_{p-3}) \stackrel{\text{def}}{=} g''(z)$ is also a polynomial in the variables $u_1, \ldots, u_{p-3}$. Then, set $u_{p-1}(z) \stackrel{\text{def}}{=} \frac{1}{g(z)}$ so that $u_{p-1}'(z) = -\frac{g'(z)}{g(z)^2} = \Phi_{p-1}(u_{p-2}, u_{p-1}) \stackrel{\text{def}}{=} -u_{p-2}u_{p-1}^2$, which is once again a polynomial. Finally, define $u_p(z)$ as the unique of the IVP $u_p'(z) = \frac{g'(z)}{g(z)} = \Phi_p(u_{p-2}, u_{p-1}) \stackrel{\text{def}}{=} u_{p-2}u_{p-1}$ with initial condition $u_p(z_0) = 0$. This construction leads to the p-dimensional polynomial complex system of ODEs $u'(z) = \Phi(u(z))$, with initial condition $u(z_0)$ fixed by the definition of the intermediate variables. For instance, $u_1(z_0) = 1/z_0$, $u_2(z_0) = \log(z_0)$, $u_3(z_0) = z_0^\alpha, \ldots, u_{p-2}(z_0) = g'(z_0)$, $u_{p-1}(z_0) = \frac{1}{g(z_0)}$ and $u_p(z_0) = 0$. Note that the number of ODEs p will depend on the map f.

Let $u_0 \stackrel{\text{def}}{=} u(z_0)$ and denote by $D_\nu(z_0) \subset \mathbb{C}$ the disk of radius $\nu > 0$ centered at z_0. Assume that the unique solution of the IVP

$$u'(z) = \Phi(u(z)), \quad u(z_0) = u_0 \tag{24}$$

is analytic on $D_\nu(z_0)$ and has been rigorously computed for all $z \in D_\nu(z_0)$ (e.g. using a Taylor series

expansion and the method of Section 3.2.1), the value of the contour integral (23) can be easily obtained, as we now demonstrate.

Suppose we fix a C^1 parameterization $\gamma : [0,1] \to \mathbb{C}$ of our contour γ, satisfying $\gamma(0) = z_0$ and $\gamma(1) = z_1$. In what follows, Log will denote a branch of the complex logarithm that is analytic on a neighbourhood of $\{g(\gamma(t)) : t \in [0,1]\}$. Let $\nu > 0$ be such that $|\gamma(t) - z_0| \leq \nu$. Then

$$\int_\gamma \frac{g'(z)}{g(z)} dz = \int_0^1 \frac{g'(\gamma(t))}{g(\gamma(t)} \gamma'(t) dt = \int_0^1 \frac{d}{dt} \operatorname{Log}(g(\gamma(t))) dt.$$

If $z \mapsto \operatorname{Log}(g(z))$ is analytic on $B_r(z_0)$, then using the Fundamental Theorem of Calculus,

$$\int_\gamma \frac{g'(z)}{g(z)} dz = \operatorname{Log}(g(z_1)) - \operatorname{Log}(g(z_0)).$$

Since u_p solves $u_p'(z) = \frac{g'(z)}{g(z)}$ with $u_p(z_0) = 0$, then $u_p(z) = \operatorname{Log}(g(z)) - \operatorname{Log}(g(z_0))$, and therefore, we conclude that

$$\int_\gamma \frac{g'(z)}{g(z)} dz = u_p(z_1). \tag{25}$$

To evaluate rigorously the value of $u_p(z_1)$ in (25), we solve rigorously the IVP (24) using Taylor series and rigorous numerics, and evaluate the last component of the solution at the point $z_1 \in D_\nu(z_0)$ in the domain of convergence of the Taylor series. We present this approach in detail in the next section.

3.2.1 Solving rigorously the complex valued IVP

Recall that we aim at solving the IVP

$$u'(z) = \Phi(u(z)), \quad u(z_0) = u_0,$$

where the vector field $\Phi : \mathbb{C}^p \to \mathbb{C}^p$ is a polynomial vector field.

For numerical stability, we choose to translate z_0 to the origin and rescale the domain (in order to have a fast geometric decay rate of the Taylor coefficients). More precisely, given a number $\nu > 0$, we map the disk $D_\nu(z_0)$ to $D_1(0)$ letting

$$\tilde{u}(z) \stackrel{\text{def}}{=} u(\nu z + z_0) \tag{26}$$

which satisfies the rescaled IVP

$$\tilde{u}'(z) = \nu \Phi(\tilde{u}(z)), \quad \tilde{u}(0) = u_0. \tag{27}$$

For each $j = 1, \ldots, p$, expand each $\tilde{u}_j$ via a Taylor series

$$\tilde{u}_j(z) = \sum_{n \geq 0} (a_j)_n z^n$$

with the associate sequence of Taylor coefficients $a_j = ((a_j)_n)_{n \geq 0}$. Denote $a = (a_1, \ldots, a_p)$ and $\phi(a) = (\phi_1(a), \ldots, \phi_p(a))$, where each $\phi_j(a)$ is exactly given by $\Phi_j(u)$, where the u_k's are replaced by a_k's and where standard products between functions are replaced by Cauchy products between sequences of Taylor coefficients. Plugging the Taylor series in the rescaled IVP (27) leads to having to solve the recursion formula

$$\begin{aligned} (a_j)_0 &= (u_0)_j \\ (a_j)_n &= \frac{\nu}{n} (\phi_j(a))_{n-1}, \quad \text{for all } n \geq 1, \end{aligned} \tag{28}$$

for each $j = 1, \dots, p$. Denote the Banach space

$$\ell^1 = \left\{ c = (c_n)_{n\geq 0} : c_n \in \mathbb{C} \text{ and } \|c\|_1 \stackrel{\text{def}}{=} \sum_{n\geq 0} |c_n|, \infty \right\} \tag{29}$$

and note that $(\ell^1, *)$ is a Banach algebra under the Cauchy product $* : \ell^1 \times \ell^1 \to \ell^1$ (that is $\|c_1 * c_2\|_1 \leq \|c_1\|_1 \|c_2\|_1$ for all $c_1, c_2 \in \ell^1$). The Banach space we consider for the computer-assisted proofs is a product space of p copies of ℓ^1. We first consider a single copy of ℓ^1. For any $N \in \mathbb{N}$ we define the projection

$$(\pi_N^1 c)_n \stackrel{\text{def}}{=} \begin{cases} c_n & \text{for } 0 \leq n \leq N, \\ 0 & \text{for } n > N, \end{cases} \qquad \text{for any } c \in \ell^1.$$

The projection on the (natural) complement is denoted by

$$\pi_\infty^1 c \stackrel{\text{def}}{=} c - \pi_N^1 c.$$

We extend these projections to

$$(\ell^1)^p = \left\{ a = (a_1, \dots, a_p) \mid a_j \in \ell^1 \text{ for } j = 1, \dots, p \right\}$$

by setting

$$\pi_N a \stackrel{\text{def}}{=} (\pi_N^1 a_1, \dots, \pi_N^1 a_p) \quad \text{for any } a \in (\ell^1)^p,$$

and $\pi_\infty = I_{(\ell^1)^p} - \pi_N$.

The ranges of the projections π_N and π_∞ are

$$\begin{aligned} X_N^p &= \left\{ a \in (\ell^1)^p \mid (a_j)_n = 0 \text{ for any } n > N \text{ and all } j = 1, \dots, p \right\}, \\ X_\infty^p &= \left\{ a \in (\ell^1)^p \mid (a_j)_n = 0 \text{ for all } 0 \leq n \leq N \text{ and all } j = 1, \dots, p \right\}. \end{aligned}$$

The subspace X_N^p can be identified with $(\mathbb{R}^{N+1})^p \simeq \mathbb{R}^{p(N+1)}$. Similarly, we define

$$\begin{aligned} X_N^1 &= \left\{ c \in \ell^1 : c_n = 0 \text{ for any } n > N \right\}, \\ X_\infty^1 &= \left\{ c \in \ell^1 : c_n = 0 \text{ for all } 0 \leq n \leq N \right\}. \end{aligned}$$

Define the Banach space $X \stackrel{\text{def}}{=} (\ell^1)^p = \ell^1 \times \cdots \times \ell^1$ which we endow with the norm

$$\|a\|_X = \max_{1\leq j\leq p} \|a_j\|_1. \tag{30}$$

We note that since X_∞^p is a closed linear subspace of X it is a Banach space with the norm (30).

The projections onto the components of $a = (a_1, \dots, a_p) \in (\ell^1)^p$ are denoted by

$$\pi^j a = a_j \quad \text{for } j = 1, \dots, p.$$

Define the component-wise *shift* operator $S : \ell^1 \to \ell^1$ by

$$(Sc)_n = \begin{cases} 0 & \text{if } n = 0 \\ c_{n-1} & \text{if } n \geq 1. \end{cases} \tag{31}$$

and the *integration operator* $\Lambda_N : X_\infty^1 \to X_\infty^1$ defined component-wise by

$$(\Lambda_N c)_n = \begin{cases} 0 & \text{if } 0 \leq n \leq N, \\ \frac{1}{n} c_n & \text{if } n \geq N+1. \end{cases} \tag{32}$$

The proof of the following lemma concerning the norms of these operators is elementary and omitted.

Lemma 8. *For fixed N,*

$$\|\pi_N\|_{B(X,X)} = \|\pi_\infty\|_{B(X,X)} = 1, \qquad \|S\|_{B(\ell^1,\ell^1)} = 1, \qquad \|\Lambda_N\|_{B(X^1_\infty,X^1_\infty)} = \frac{1}{N+1}.$$

Finally, we note that since X^1_∞ is a subspace of ℓ^1 the operator Λ_N may also be interpreted as mapping X^1_∞ into ℓ^1. Likewise, π^1_∞ may be interpreted as mapping from ℓ^1 to X^1_∞.

For each $j = 1, \dots, p$, let

$$F_j(a) = \{(F_j(a))_n\}_{n\geq 0}$$

be defined component-wise by

$$(F_j(a))_n \stackrel{\text{def}}{=} \begin{cases} (a_j)_0 - (u_0)_j & \text{if } n = 0, \\ (a_j)_n - \frac{\nu}{n}(\phi_j(a))_{n-1} & \text{if } n \geq 1. \end{cases} \tag{33}$$

The first term is imposed by the initial condition $x_n(0) = a_{n,0} = x_{0,n}$.

We introduce $\Psi : X \to X$ defined component-wise by

$$\begin{aligned} (\Psi_j(a))_0 &\stackrel{\text{def}}{=} (a_j)_0 - (F_j(a))_0 = (u_0)_j \\ (\Psi_j(a))_n &\stackrel{\text{def}}{=} (a_j)_n - (F_j(a))_n = \frac{\nu}{n}(\phi_j(a))_{n-1} \quad \text{for } n \geq 1. \end{aligned}$$

Clearly fixed points of Ψ correspond to zeros of F. We assume that we have computed through recursion

$$(\bar{a}_j)_n = (\Psi_j(\bar{a}))_n \quad \text{for all } n = 0, \dots, N \text{ and } j = 1, \dots, p. \tag{34}$$

In other words, $\bar{a} \stackrel{\text{def}}{=} (\bar{a}_1, \dots, \bar{a}_p) \in X^p_N$ is the solution of $\pi_N F(a) = 0$. We seek a fixed point $\tilde{u} \in X^p_\infty$ of $T : X^p_\infty \to X^p_\infty$ defined by

$$T(v) \stackrel{\text{def}}{=} \pi_\infty \Psi(\bar{a} + v), \tag{35}$$

given component-wise by

$$\pi^j T(v) = \nu \Lambda_N \pi^1_\infty S(\phi_j(\bar{a} + v)), \qquad j = 1, \dots, p. \tag{36}$$

More precisely if $\tilde{v} \in X^p_\infty$ is a fixed point of T given in (35), then $\tilde{a} \stackrel{\text{def}}{=} \bar{a} + \tilde{v} \in X$ solves $F(\tilde{a}) = 0$, and by construction $\tilde{a} = (\tilde{a}_1, \dots, \tilde{a}_p)$ provides the sequence of Taylor coefficients of the solution $\tilde{v} = (\tilde{v}_1, \dots, \tilde{v}_p)$ of the rescaled IVP (27) on some domain $D_1(0)$. This in turn provides, via the rescaling (26), the sequence of Taylor coefficients of the solution $u = (u_1, \dots, u_p)$ of the IVP (24) on some domain $D_\nu(z_0)$. Given any $z_1 \in D_\nu(z_0)$, the value of the p^{th} component of the solution at z_1 can finally be evaluated to obtain a rigorous (and tight) enclosure for the value of the contour integral in (25).

The following theorem will be used to prove the existence of a fixed point of T, together with rigorous error bounds.

Theorem 9. *Let $Y_0 \geq 0$ and $Z\colon (0,\infty) \to [0,\infty)$ a non-negative function satisfying that*

$$\|T(0)\|_X \leq Y_0, \tag{37}$$

and

$$\sup_{v \in \overline{B_r(0)}} \|DT(v)\|_{B(X^p_\infty, X^p_\infty)} \leq Z(r). \tag{38}$$

Define the radii polynomial

$$p(r) \stackrel{\text{def}}{=} Z(r)r - r + Y_0. \tag{39}$$

If there exists $r_0 > 0$ such that $p(r_0) < 0$, then there exists a unique $\tilde{v} \in \overline{B_{r_0}(0)}$ so that $T(\tilde{v}) = \tilde{v}$.

The computation of the bounds Y_0 and $Z(r)$ are rather standard in the field of rigorous numerics and rather than providing general formulas for them, we instead construct them explicitly in the context of the example of Section 4.3.2. We are ready to present a procedure to compute rigorously the contour integration.

3.2.2 Procedure for the rigorous contour integration

In this short section, we present a step-by-step algorithmic approach to the rigorous contour integration.

- Fix the origin of the path $z_0 \in \gamma$.
- Fix N the order of the Taylor series approximation for a_j $(j = 1, \dots, p)$.
- Fix $\nu = 1$ and compute rigorously (with interval arithmetic) the first $N+1$ Taylor coefficients $((\bar{a}_j^1)_n)_{n=0}^N$ of each $u_j(z)$ using the recursion formula (28). At this point, note that the Taylor coefficients may not decay, but rather increase (this of course depends on the radius of convergence of the Taylor series).
- Adjust the scaling $\nu > 0$ such that the last Taylor coefficient of u_p reaches the wanted precision, while making sure that the new resulting Taylor coefficients are still solving the recursion formula (28) for ν. This can easily be done simply by rescaling $(\bar{a}_j^1)_n$ to $(\bar{a}_j^1)_n \nu^n$. In practice, we choose ν such that

$$|(\bar{a}_p^1)_N|\nu^N = 10^{-10} \iff \ln(|(\bar{a}_p^1)_N|) + N\ln(\nu) = -10\ln(10) \iff \nu = e^{-\frac{10\ln(10)+\log(|(\bar{a}_p^1)_N|)}{N}}.$$

  The new resulting coefficients $(\bar{a}_j)_n \overset{\text{def}}{=} (\bar{a}_j^1)_n \nu^n$ $(n = 0, \dots, N$ and $j = 1, \dots, p)$ provide a solution of IVP (27) with $\nu > 0$ and satisfy $|(\bar{a}_p)_N| = 10^{-10}$. Denote

$$u_j^{(N)}(z) \overset{\text{def}}{=} \sum_{n=0}^{N} (\bar{a}_j)_n z^n,$$

- Compute the bounds Y_0 and $Z(r)$ of Theorem 9 using interval arithmetic, define $p(r)$ as in (39) and verify if it is possible to find $r_0 > 0$ such that $p(r_0) < 0$. If not, decrease ν, rescale once again the Taylor coefficients and attempt again to verify the hypothesis of Theorem 9. Note that this will work eventually for ν sufficiently small.
- Denote by r_{min} the *smallest* radius for which the proof works and denote $\tilde{v} = (\tilde{v}_1, \dots, \tilde{v}_p) \in \overline{B_{r_{min}}(0)}$ the fixed point of T and $\tilde{a} = \bar{a} + \tilde{v}$ the true solution. Denote the true solution of the IVP (27) by

$$\tilde{u}_j(z) = u_j^{(N)}(z) + \sum_{n>N} (\tilde{v}_j)_n z^n = \sum_{n=0}^{N} (\bar{a}_j)_n z^n + \sum_{n>N} (\tilde{v}_j)_n z^n = \sum_{n\geq 0} (\tilde{a}_j)_n z^n.$$

- From the proof, we get that for each $j = 1, \dots, p$,

$$\begin{aligned}\sup_{z\in\overline{D_1(0)}} \left| u_j(z) - u_j^{(N)}(z) \right| &= \sup_{z\in\overline{D_1(0)}} \left| \sum_{n=0}^{\infty} (\tilde{a}_i)_n z^n - \sum_{n=0}^{N} (\bar{a}_i)_n z^n \right| \\ &= \sup_{z\in\overline{D_\nu(z_0)}} \left| \sum_{n=0}^{\infty} (\tilde{a}_i)_n \left(\frac{z-z_0}{\nu}\right)^n - \sum_{n=0}^{N} (\bar{a}_i)_n \left(\frac{z-z_0}{\nu}\right)^n \right| \leq r_{min}.\end{aligned}$$

- Take $z_1 \in \gamma$ such that $\frac{|z_1 - z_0|}{\nu} = 1$, recall (25) and evaluate the rigorous enclosure with interval arithmetics

$$\int_\gamma \frac{g'(z)}{g(z)} dz = \tilde{u}_p(z_1) \overset{\text{def}}{=} \sum_{n\geq 0} (\tilde{a}_p)_n \left(\frac{z_1 - z_0}{\nu}\right)^n \in \sum_{n=0}^{N} (\bar{a}_p)_n \left(\frac{z-z_0}{\nu}\right)^n + \delta, \tag{40}$$

  where $\delta \overset{\text{def}}{=} [-r_{min}, r_{min}]$.

At the end of one computation using the above step-by-step procedure, we let $z_0 \stackrel{\text{def}}{=} z_1$ and start over, until we have computed all contour integrals in (22). Recall that $\Gamma = \bigcup_{k=1}^{m} \gamma_k$. For each $k = 1, \ldots, m$, use (40) and denote the rigorous enclosure of $\int_{\gamma_k} \frac{g'(z)}{g(z)}\, dz$ by

$$\int_{\gamma_k} \frac{g'(z)}{g(z)}\, dz \in S_k + \delta_k \stackrel{\text{def}}{=} \sum_{n=0}^{N} (\bar{a}_p)_n \left(\frac{z - z_0}{\nu}\right)^n + \delta_k,$$

with $\delta_k \stackrel{\text{def}}{=} [-r^k_{min}, r^k_{min}]$. Finally the rigorous enclosure of the number of zeros is

$$N_{\text{zeros}} \in \frac{1}{2\pi i} \left(\sum_{k=1}^{m} S_k + [-1, 1] \sum_{k=1}^{m} r^k_{min} \right). \tag{41}$$

If the rigorous enclosure of N_{zeros} provided by (41) contains a unique integer, then we have our rigorous count.

4 Computer-assisted proofs

This section contains outlines of the computer-assisted proofs of Theorem 2, Theorem 3 and Theorem 4. The enclosures of zeroes provided in those theorems are computed from the numerical outputs of the proofs, which appear in Table 1, Table 2 and Table 3. The codes to complete the proofs are available at [12].

4.1 Proof of Theorem 2

First, we scale time to make the delay a smooth parameter. Let $\hat{t} = t\tau$. Completing the change of variables and dropping the hats, we get the delay equation

$$\dot{y} = \tau(-\sigma y(t) + e^{-y(t-1)}).$$

We now treat τ as the parameter and $\sigma \in \{0.3, 0.35\}$ as a fixed constant, since the delay is now equal to 1. We automatically prove the theorem by running the MATLAB function `prove_single_delay_examples.m` with the input `NUMBER` set to 1 for the first proof ($\sigma = 0.3$) and 2 for the second ($\sigma = 0.35$). This function calls `prove_Hopf_isolation.m` as outlined in Section 2.3 to verify the hypotheses of Theorem 6. To check the non-resonance and simplicity, we use the generalized Morse index approach, making use of `prove_non_resonance.m` for the verification of $\mu_{1-\delta_1} - \mu_{1+\delta_2} = 2$. The parameters used in the proof and associated outputs appear in Table 1.

4.2 Proof of Theorem 3

The setup for Theorem 3 is even more straightforward than the previous one. The only important difference is that since the system is two-dimensional, we fix the first component of the eigenvector v to $v_1 = 1$. The coupling ξ is treated as the bifurcation parameter and we run `prove_single_delay_examples.m` with the input `NUMBER` set to 3 (for $\rho = 0$) or 4 (for $\rho = 1$). This function calls `prove_Hopf_isolation.m` as outlined in Section 2.3 to verify the hypotheses of Theorem 6. To check the non-resonance and simplicity, we use the generalized Morse index approach, making use of `prove_non_resonance.m` for the verification of $\mu_{1-\delta_1} - \mu_{1+\delta_2} = 2$. The parameters used in the proof and associated outputs appear in Table 2, and the eigenvalues at the bifurcation point can be visualized with Figure 2.

	$\sigma = 0.3$	$\sigma = 0.35$
x_0	1.104542018324	1.025065556445
x_0'	0	0
α_0	19.208854104207	37.030171112739
ω_0	-2.703005650033	-2.919994153135
$\mathrm{Re}(\lambda')$	0.007171184698	0.001131897009
$\mathrm{Im}(\lambda')$	-0.017941603965	-0.005411625903
r_0	$7.1870665 \times 10^{-13}$	$9.7779366 \times 10^{-13}$
δ_1	0.1	0.094
δ_2	0.1	0.3
ν	1.15	1.06
N	100	490
$C(1-\delta_1)$	0.91823	0.98829
$C(1+\delta_2)$	0.89056	0.16294
$\mu_{1-\delta_1}$	2	2
$\mu_{1+\delta_2}$	0	0

Table 1: Top portion: Candidate zero $(x_0, \ldots, \mathrm{Im}(\lambda'))$ and uniqueness radius r_0 (rounded up for readability) for the Hopf bifurcation isolation proofs of the Lasota-Wazewska-Czyzewska equation. Note that the eigenvector v is fixed to $v = 1$, and the bifurcation parameter τ corresponds to the component α in the coordinates of the zero. Bottom portion: Parameters $(\delta_1, \delta_2, \nu, N)$ used for the Morse index computations, product C of the technical bounds C_1, C_2 and C_3 for the indices $\mu_{1-\delta_1}$ and $\mu_{1+\delta_2}$, and these indices.

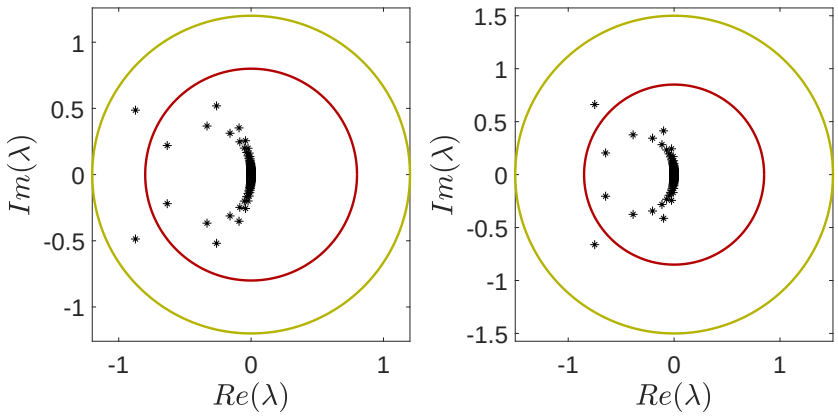

Figure 2: Eigenvalues of the step map at the bifurcation point for the coupled Lasota-Wazewska-Czyzewska equations. The circles in red and green have radius $1 - \delta_1$ and $1 + \delta_2$ respectively, and the two eigenvalues in the gap correspond to the imaginary eigenvalues $\pm i\omega_0$ from Table 2. Left: $\rho = 0$. Right: $\rho = 1$. The proof for $\rho = 0$ is more computationally expensive because, compared to $\rho = 1$, there are more eigenvalues closer to the unit circle.

	$\rho = 0$	$\rho = 1$
x_0	1.144668868008599	1.585823613805185
y_0	1.084122019684906	0.903053550980479
x_0'	-1.919211635684326	-1.727579568874282
y_0'	0.957842795546628	0.581589081774491
α_0	0.178097289316629	0.067660704405282
ω_0	-0.154904637991545	-0.142261377213083
$\mathrm{Re}(v_2)$	0.868760285342032	0.208874995011447
$\mathrm{Im}(v_2)$	-0.041065942913387	-0.099748188056958
$\mathrm{Re}(\lambda')$	-0.047501861871352	-0.008458308451281
$\mathrm{Im}(\lambda')$	-0.073744885404130	-0.149652361211147
$\mathrm{Re}(v_2')$	4.238789580398924	2.225857970381196
$\mathrm{Im}(v_2')$	-6.020231755626770	-2.762306284945626
r_0	$7.0027385 \times 10^{-14}$	$1.8492517 \times 10^{-13}$
δ_1	0.05	0.15
δ_2	0.1	0.5
ν	1.12	1.15
N	280	150
$C(1-\delta_1)$	0.90069	0.95435
$C(1+\delta_2)$	0.29771	0.19048
$\mu_{1-\delta_1}$	2	2
$\mu_{1+\delta_2}$	0	0

Table 2: Top portion: Candidate zero $(x_0, y_0, \ldots, \mathrm{Re}(v_2'), \mathrm{Im}(v_2'))$ and uniqueness radius r_0 (rounded up for readability) for the Hopf bifurcation isolation proofs of the coupled Lasota-Wazewska-Czyzewska equations. Note that the first component of the eigenvector v is fixed to $v_1 = 1$, and the bifurcation parameter ξ corresponds to the component α in the coordinates of the zero. Bottom portion: Parameters $(\delta_1, \delta_2, \nu, N)$ used for the Morse index computations, product C of the technical bounds, and the indices $\mu_{1-\delta_1}$ and $\mu_{1+\delta_2}$.

4.3 Proof of Theorem 4

If we substitute the kernel ϕ from (6) into the PDE (4) we get

$$u_t = Du_{xx} + \mu u\left(\sigma - \frac{h}{N_1}\int_{-N_1}^{0} u(t,x-y)dy - \frac{1-h}{N_2}\int_{0}^{N_2} u(t,x-z)dz\right).$$

We make the change of variables $u(t,x) = w(DN_1^{-2}t, N_1^{-1}x)$ and define new parameters $\rho = \mu N_1^2 D^{-1}$ and $M = \frac{N_2}{N_1}$. We get

$$w_t = w_{xx} + \rho w\left(\sigma - h\int_{-1}^{0} w(t,x-y)dy - \frac{1-h}{M}\int_{0}^{M} w(t,x-z)dz\right). \tag{42}$$

Suppose $w(t,x) = \psi(x+ct)$ for a wave profile ψ and speed c. Substituting this into (42), we get the functional differential equation

$$c\psi'(t) = \psi''(t) + \rho\psi(t)\left(\sigma - h\int_{-1}^{0} \psi(t-y)dy - \frac{1-h}{M}\int_{0}^{M} \psi(t-z)dz\right) \tag{43}$$

for the wave profile. The remaining steps of the proof are completed by running the MATLAB function `prove_Twave_Hopf.m`. This function takes two inputs (j,k) and completes the proof Wj from Theorem 4 for the wave velocity c_k. We will now outline the steps that this function completes and state the numerical outputs of the proof.

4.3.1 Hopf isolation and transersality conditions

Define $f : C([-M,1],\mathbb{R}^2)\times\mathbb{R} \to C([-M,1],\mathbb{R}^2)$ by

$$f(q,c) = \begin{bmatrix} q_2(0) \\ cq_2(0) - \rho q_1(0)\left(1 - h\int_{-1}^{0} q_1(-s)ds - \frac{1-h}{M}\int_{0}^{M} q_1(-s)ds\right) \end{bmatrix}.$$

Defining $(q_1,q_2) = (\psi,\psi')$, the equation (43) is equivalent to $\dot{q} = f(q,c)$ and therefore has a fixed point at $(\sigma,0) = (1,0)$. We use Theorem 6 and Theorem 7 to verify the isolation and transversality conditions (1.) and (2.) from Theorem 1. To do this, we need to compute a few partial differentials. Letting $x,y,w \in C([-M,1],\mathbb{R}^2)$,

$$\begin{aligned}
D_1 f(x,c)y &= \begin{bmatrix} y_2(0) \\ cy_2(0) - \rho y_1(0)\left(\sigma - h\int_{-1}^{0} x_1(-s)ds - \frac{(1-h)}{M}\int_{0}^{M} x_1(-s)ds\right) \\ \quad + \rho x_1(0)\left(h\int_{-1}^{0} y_1(-s)ds + \frac{(1-h)}{M}\int_{0}^{M} y_1(-s)ds\right) \end{bmatrix} \\
D_2 f(x,c) &= \begin{bmatrix} 0 \\ x_2(0) \end{bmatrix} \\
D_1^2 f(x,c)[y,w] &= \begin{bmatrix} 0 \\ \rho y_1(0)\left(h\int_{-1}^{0} w_1(-s)ds + \frac{(1-h)}{M}\int_{0}^{M} w_1(-s)ds\right) \\ \quad + \rho w_1(0)\left(h\int_{-1}^{0} y_1(-s)ds + \frac{(1-h)}{M}\int_{0}^{M} y_1(-s)ds\right) \end{bmatrix} \\
D_2 D_1 f(x,c)y &= \begin{bmatrix} 0 \\ y_2(0) \end{bmatrix}.
\end{aligned}$$

	W1	W2	W3	W4
c_1	-0.499960441060187	0.499960441060186	-0.363754795740408	0.743510960061904
ω_0	4.637215079560793	4.637215079560793	4.592098499884637	2.889763462936531
$\mathrm{Re}(v_2)$	0	0	0	0
$\mathrm{Im}(v_2)$	4.637215079560793	4.637215079560793	4.592098499884637	2.889763462936531
$\mathrm{Re}(\lambda')$	0.070132958310718	0.048464565698432	0.040085041058377	-0.057440819946235
$\mathrm{Im}(\lambda')$	0.216934012587930	0.183223000908009	0.196850686215880	0.052484450151143
$\mathrm{Re}(v_2')$	1.076102632753096	0.898109028431434	0.944042781931582	0.094226826472853
$\mathrm{Im}(v_2')$	-0.108287599264741	-0.041517613973126	0.012776229303893	0.218474832912888
r_0	$2.5496855 \times 10^{-15}$	$3.2214306 \times 10^{-15}$	$4.0559742 \times 10^{-15}$	$2.5866136 \times 10^{-15}$

	W1	W2	W3	W4
c_2	-1.407518070559178	1.407518070559176	0.225343700115205	38.377317897727600
ω_0	3.648913186685016	3.648913186685016	3.513777373551947	1.612796341206019
$\mathrm{Re}(v_2)$	0	0	0	0
$\mathrm{Im}(v_2)$	3.648913186685016	3.648913186685016	3.513777373551947	1.612796341206019
$\mathrm{Re}(\lambda')$	0.111230975589598	0.103152903698957	0.094953411313056	0.025059472072250
$\mathrm{Im}(\lambda')$	0.048288669938503	0.054733236581360	0.050485616225114	0.003084428687102
$\mathrm{Re}(v_2')$	0.287432140095682	0.302869732410634	0.272348627294689	0.030034027373518
$\mathrm{Im}(v_2')$	-0.357583503658218	-0.321662753970615	-0.283159531988272	-0.037331396183577
r_0	$5.6381454 \times 10^{-15}$	$7.5708092 \times 10^{-15}$	$5.8092945 \times 10^{-15}$	$1.3536766 \times 10^{-15}$

Table 3: Candidate zeroes for the Hopf isolation and transversality part of the proof of Theorem 4 and radius from the radii polynomial. The parameter is $\alpha = c_1$, and the steady state is fixed at $x_0 = (1, 0)$, so $x_0' = (0, 0)$ in terms of the variables of Theorem 6. The first component of the eigenvector v is fixed to $v_1 = 1$. Top: the wave with velocity near c_1. Bottom: the wave with velocity near c_2. We have rounded up the expressions of r_0 for readability.

The MATLAB function `prove_Twave_Hopf_isolation.m` generates (if not yet done) a symbolic representation of F, a symbolic representation of the Fréchet derivative DF, and Taylor expansions using a routine formally analogous to the one in Section 2.3 for the case of a single discrete delay. It then implements the radii polynomial from Theorem 7 using the bound Z_2 from (16) and automatically checks the transversality condition $\mathrm{Re}(\lambda') \neq 0$. The symbolic calculations are a bit slow and result in inefficient function files that must then be passed interval data, so the code takes a few seconds to run rather than being nearly instant. The result is that the zero-isolation conditions of Theorem 6 are automatically checked. The approximate zeroes that are passed as the inputs to the proof and the resulting outputs are provided in Table 3.

4.3.2 Non-resonance and simplicity

Before we begin, we emphasize that the radius r_0 from the previous Hopf isolation and transversality section are propagated into this proof. The result is that we replace c with the `midrad(c,r_0)` in any subsequent computations. This will not be explicitly written in what follows.

Linearizing at the steady state $\psi = 1$, we get

$$cv'(t) = v''(t) - \rho h \int_{-1}^{0} v(t-y)dy - \rho \frac{1-h}{M} \int_{0}^{M} v(t-z)dz. \tag{44}$$

Note that the parameter σ does not appear in the linearization. If we now make the eigenvalue ansatz

$v = e^{t\lambda}$, we get (after some simplifications) the equation

$$\lambda^2 - c\lambda + \frac{\rho}{\lambda}\left(h(1-e^{\lambda}) + \frac{1-h}{M}(e^{-M\lambda}-1)\right) = 0. \tag{45}$$

If $\lambda = i\omega$, then (45) reduces to

$$0 = -\omega^2 + i\omega c - \frac{1}{\omega} i\rho \left(h(1-\cos\omega - i\sin\omega) + \frac{1-h}{M}(\cos(\omega M) - i\sin(\omega M) - 1)\right),$$

which we can equivalently write as

$$\omega^3 = i\omega^2 c - i\rho\left(h(1-\cos\omega - i\sin\omega) + \frac{1-h}{M}(\cos(\omega M) - i\sin(\omega M) - 1)\right) \tag{46}$$

Define

$$\hat{\omega} = \sqrt[3]{\rho\left(h + \frac{1-h}{M}\right)}.$$

Taking real parts and absolute values in (46), it follows that

$$|\omega|^3 = \rho\left(h|\sin\omega| + \frac{1-h}{M}|\sin(\omega M)|\right) \leq \rho\left(h + \frac{1-h}{M}\right) = \hat{\omega}^3, \tag{47}$$

from which we conclude that $|\omega| \leq \hat{\omega}$.

Now, making the transformation $z = e^{\lambda}$ in (45) and multiplying the result by $\log(z)$, zeroes z satisfy the equation

$$g(z) \stackrel{\text{def}}{=} \log(z)^3 - c\log(z)^2 + \rho\left(h(1-z) + \frac{1-h}{M}(z^{-M}-1)\right) = 0. \tag{48}$$

We use the rigorous contour integral method from Section 3.2 to evaluate

$$\oint_{\Gamma} \frac{g'(z)}{g(z)} dz$$

over the contour Γ that bounds the rectangle in polar coordinates given by

$$(r,\theta) \in [1-\Delta r, 1+\Delta r] \times [-\epsilon, \hat{\omega}+\epsilon],$$

where $\hat{\omega}$ is the bound defined by (47) and $\Delta r = 0.09$ and $\epsilon = 0.05$ are two positive parameters that we have selected to ensure the contour both strictly includes (by our choice of ϵ) $z = 1 \in \mathbb{C}$ and $e^{i\hat{\omega}}$, as well as ensuring that no extraneous zeroes close to the unit circle are include (by choice of Δr).

Note that this contour must enclose *any* $z = e^{i\omega}$ for which $\lambda = i\omega$ and $\omega > 0$ is a solution of the characteristic equation (45), due to the inequality (47). Our goal is to prove that this contour contains exactly two zeroes of g: one at $z = 1$ that comes from the multiplication we made by $\log(z)$, and the other being $z = e^{i\omega_0}$ for $\omega_0 > 0$ coming from the Hopf bifurcation. For the function g in (48), the associated polynomial embedding is given by

$$u'(z) = \Phi(u(z)) \stackrel{\text{def}}{=} \begin{pmatrix} -u_1^2 \\ u_1 \\ -Mu_1u_3 \\ -3u_1^2u_2^2 + (6+2c)u_1^2u_2 - 2cu_1^2 + \rho(1-h)(M+1)u_1^2u_3 \\ -u_4u_5^2 \\ u_4u_5 \end{pmatrix} \tag{49}$$

with initial condition

$$u(z_0) = \begin{pmatrix} 1/z_0 \\ \log(z_0) \\ z_0^{-M} \\ g'(z_0) \\ \frac{1}{g(z_0)} \\ 0 \end{pmatrix}. \tag{50}$$

By construction, $u_6'(z) = \frac{g'(z)}{g(z)}$. To make use of the radii polynomial approach and apply Theorem 9 to rigorously compute u_6 along various points on the contour γ, we need explicit formulas for the bounds. This is accomplished with the following.

Theorem 10. *Fix $N \in \mathbb{N}$. Let $\bar{a} \in X_N$ solve the recurrence relation* (34) *up to order N. Setting*

$$Y_0 \stackrel{\text{def}}{=} \max_{1\le j\le 6} \sum_{n=N}^{4N} \frac{\nu}{n+1} |(\phi_j(\bar{a}))_n|, \tag{51}$$

then (37) *holds. Setting $\beta_1 \stackrel{\text{def}}{=} 6+2c$, $\beta_3 \stackrel{\text{def}}{=} \rho(1-h)(M+1)$,*

$$\begin{aligned} z_0 \stackrel{\text{def}}{=} \max\big\{ & 1, 2(\|\bar{a}_1\| + \|\bar{a}_2\|), 3(\|\bar{a}_1\| + \|\bar{a}_3\|), M(\|\bar{a}_1\| + \|\bar{a}_6\|), 3\|\bar{a}_3\| + 2c\|\bar{a}_2\| + |\beta_2|\|\bar{a}_6\| + (2c+3+|\beta_2|)\|\bar{a}_1\|, \\ & 6\|\bar{a}_1\|\|\bar{a}_3\| + 2|\beta_1|\|\bar{a}_1\|\|\bar{a}_2\| + 4c\|\bar{a}_1\| + 2|\beta_3|\|\bar{a}_1\|\|\bar{a}_6\| + (|\beta_1| + 3 + |\beta_3|)\,\|\bar{a}_1\|^2, \\ & \|\bar{a}_9\|^2 + 2\|u_8\|\|u_9\|, \|\bar{a}_8\| + \|\bar{a}_9\| \big\} \\ z_1 \stackrel{\text{def}}{=} \max\{ & 2M, 6 + 4c + 2|\beta_2|, 2(6 + 2|\beta_1| + 2|\beta_3|)\|\bar{a}_1\| + 6\|\bar{a}_3\| + 2|\beta_1|\|\bar{a}_2\| + 4c + 2|\beta_3|\|\bar{a}_6\|, 2\,(2\|\bar{a}_9\| + \|u_8\|)\} \\ z_2 \stackrel{\text{def}}{=} & \ 9 + 3|\beta_1| + 3|\beta_3| \\ z_3 \stackrel{\text{def}}{=} & \ 12 \end{aligned}$$

and

$$Z(r) \stackrel{\text{def}}{=} \frac{\nu}{N+1} \sum_{m=0}^{3} z_m r^m, \tag{52}$$

then (38) *holds. Moreover, if there exists $r_0 > 0$ such that $p(r_0) < 0$, then there is a $\tilde{u} \in X_\infty$ with $\|\tilde{u}\|_X \le r_0$ such that $u(z) = (u_1(z), \dots, u_6(z))$ given component-wise by*

$$u(z) \stackrel{\text{def}}{=} \sum_{n=0}^{N} (\bar{a}_j)_n z^n + \sum_{n=N+1}^{\infty} \tilde{u}_n z^n$$

solves the initial value problem (27) *for $z \in D_1(0)$.*

Proof. The construction of Y_0 follows from the fact that the vector field Φ is quartic. As for $Z(r)$, note that since

$$\Phi(u(z)) \stackrel{\text{def}}{=} \begin{pmatrix} -u_1^2 \\ u_1 \\ -Mu_1u_3 \\ -3u_1^2u_2^2 + \beta_1 u_1^2 u_2 - 2cu_1^2 + \beta_3 u_1^2 u_3 \\ -u_4u_5^2 \\ u_4u_5 \end{pmatrix}$$

then

$$D\Phi(u) = \begin{pmatrix} -2u_1 & 0 & 0 & 0 & 0 & 0 \\ 1 & 0 & 0 & 0 & 0 & 0 \\ -Mu_3 & 0 & -Mu_1 & 0 & 0 & 0 \\ -6u_1u_2^2 + 2\beta_1u_1u_2 - 4cu_1 + 2\beta_3u_1u_3 & -6u_1^2u_2 + \beta_1u_1^2 & \beta_3u_1^2 & 0 & 0 & 0 \\ 0 & 0 & 0 & -u_5^2 & -2u_4u_5 & 0 \\ 0 & 0 & 0 & u_5 & u_4 & 0 \end{pmatrix}$$

We conclude that for all $h \in B_1(0)$

$$\begin{aligned}
\|D\Phi_1(u)h\| &\leq 2\|\bar{a}_1\| + 2r \\
\|D\Phi_2(u)h\| &\leq 1 \\
\|D\Phi_3(u)h\| &\leq M(\|\bar{a}_1\| + \|\bar{a}_3\|) + 2Mr \\
\|D\Phi_4(u)h\| &\leq 6\|\bar{a}_1\|\|\bar{a}_2\|^2 + 2|\beta_1|\|\bar{a}_1\|\|\bar{a}_2\| + 4c\|\bar{a}_1\| + 2|\beta_3|\|\bar{a}_1\|\|\bar{a}_3\| + 6\|\bar{a}_1\|^2\|\bar{a}_2\| + (|\beta_1| + |\beta_3|)\|\bar{a}_1\|^2 \\
&\quad + \big(24\|\bar{a}_1\|\|\bar{a}_2\| + 6(\|\bar{a}_1\|^2 + \|\bar{a}_2\|^2) + 4c + 2(|\beta_1| + |\beta_3|)(2\|\bar{a}_1\| + \|\bar{a}_2\|)\big)r \\
&\quad + \big(18(\|\bar{a}_1\| + \|\bar{a}_2\|) + 3|\beta_1| + 3|\beta_3|\big)r^2 + 12r^3 \\
\|D\Phi_5(u)h\| &\leq \|\bar{a}_5\|^2 + 2\|\bar{a}_4\|\|\bar{a}_5\| + 2\left(\|\bar{a}_4\| + 2\|\bar{a}_5\|\right)r + 3r^2 \\
\|D\Phi_6(u)h\| &\leq \|\bar{a}_4\| + \|\bar{a}_5\| + 2r.
\end{aligned}$$

Collecting the coefficients in front of powers of r yield the polynomial bound $Z(r)$. □

The MATLAB function `fun_line_integral.m` is an implementation of these bounds and the rigorous integrator, specified to the present problem. The contour is adaptively covered by balls on which we can prove that u is analytic, and we ultimately are able to prove that the contour integral is equal to 2 and therefore, g has exactly two zeroes inside of Γ. More precisely, the number of zeroes is contained in an interval of the form $2 + [-1, 1]r_*$, where

$$r_* = \left| \frac{1}{2\pi i} \sum_{k=1}^{m} r_{min}^k \right|, \tag{53}$$

with r_{min}^k as defined in (41), and since $r_* < 1$ the number of zeroes must be precisely 2. The outputs appear in Table 4. See Figure 3 for the contours and covering by balls for two of the eight proofs.

Acknowledgments

Kevin E. M. Church acknowledges the support of NSERC through the NSERC Postdoctoral Fellowships Program. Jean-Philippe Lessard is supported by an NSERC Discovery Grant.

References

[1] AUTO. *http://indy.cs.concordia.ca/auto/*.

[2] Kate A. Abell, Christopher E. Elmer, A. R. Humphries, and Erik S. Van Vleck. Computation of mixed type functional differential boundary value problems. *SIAM Journal on Applied Dynamical Systems*, 4(3):755–781, 2005.

Proof c_1	W1	W2	W3	W4
N_1	100	100	100	150
N_3	150	150	150	150
$\oint_\Gamma$	2	2	2	2
r_*	1.3292×10^{-9}	1.7259×10^{-9}	2.9120×10^{-9}	7.9466×10^{-9}
Proof c_2	W1	W2	W3	W4
N_1	100	100	100	200
N_3	150	150	150	200
$\oint_\Gamma$	2	2	2	2
r_*	1.4359×10^{-9}	1.9546×10^{-9}	2.9993×10^{-9}	2.7631×10^{-8}

Table 4: The contour Γ is split into four "long" segments: the "outer" segment with $r = 1 + \Delta r$ and $\theta \in [-\epsilon, \hat{\omega} + \epsilon]$, a segment from with $\theta = \hat{\omega} + \epsilon$ and $r \in [1 - \Delta r, 1 + \Delta r]$, the "inner" segment with $r = 1 - \Delta r$ and $\theta \in [-\epsilon, \hat{\omega} + \epsilon]$, and the final connecting segment $\theta = -\epsilon$ and $r \in [1 - \Delta r, 1 + \Delta r]$. See Figure 3. Each of these "long" segments is adaptively subdivided. Along the first and second segment, we used a Taylor expansion of order N_1. On the third and fourth segments, we used order N_3. The value of the contour integral is given by $\oint_\gamma$ in the table, with rigorous error bound r_* from (53). The latter bound has been rounded up for readability.

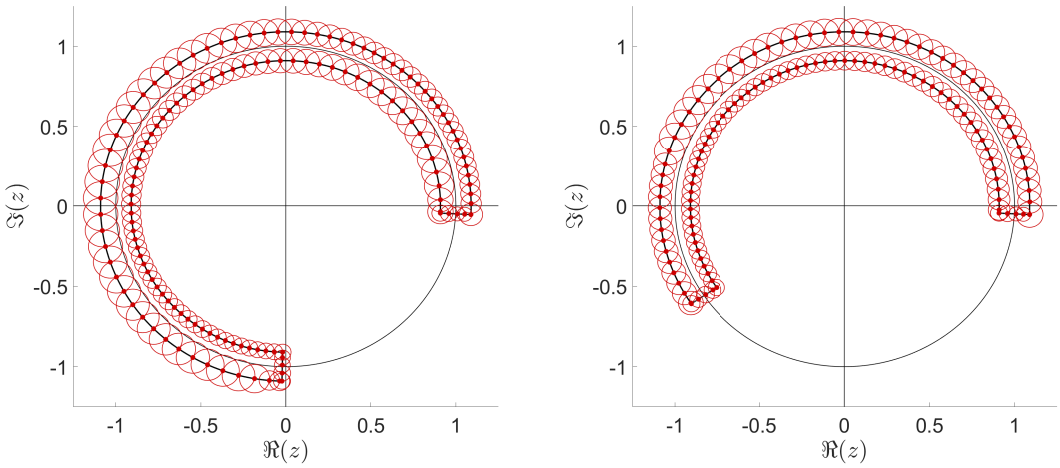

Figure 3: The contour Γ and its covering by balls of radii determined by the rigorous integrator. Left: for the proof W1 with wave velocity c_1. Right: for the proof W4 with wave velocity c_1.

[3] Herbert Amann. Hopf bifurcation in quasilinear reaction-diffusion systems. In Busenberg S. and Martelli M., editors, *Delay Differential Equations and Dynamical Systems*, number 4, pages 53–63. 1991.

[4] Gianni Arioli and Hans Koch. Computer-assisted methods for the study of stationary solutions in dissipative systems, applied to the Kuramoto-Sivashinski equation. *Arch. Ration. Mech. Anal.*, 197(3):1033–1051, 2010.

[5] Peter H. Baxendale. A stochastic Hopf bifurcation. *Probability Theory and Related Fields*, 99(4):581–616, 1994.

[6] Henri Berestycki, Grégoire Nadin, Benoit Perthame, and Lenya Ryzhik. The non-local Fisher-KPP equation: Travelling waves and steady states. *Nonlinearity*, 22(12):2813–2844, 2009.

[7] Jan Bouwe van den Berg and Jean-Philippe Lessard. Rigorous numerics in dynamics. *Notices Amer. Math. Soc.*, 62(9):1057–1061, 2015.

[8] Jan Bouwe van den Berg and Jean-Philippe Lessard, editors. *Rigorous numerics in dynamics*, volume 74 of *Proceedings of Symposia in Applied Mathematics*. American Mathematical Society, Providence, RI, 2018. AMS Short Course: Rigorous Numerics in Dynamics, January 4–5, 2016, Seattle, Washington.

[9] Jan Bouwe van den Berg, Jean-Philippe Lessard, and Elena Queirolo. Rigorous verification of Hopf bifurcations via desingularization and continuation. Preprint, 2020.

[10] Jan Bouwe van den Berg and Elena Queirolo. Rigorous validation of a Hopf bifurcation in the Kuramoto-Sivashinsky PDE. Preprint, 2020.

[11] Roberto Castelli and Jean-Philippe Lessard. A method to rigorously enclose eigenpairs of complex interval matrices. *Conference Applications of Mathematics 2013 in honor of the 70th birthday of Karel Segeth. Institute of Mathematics AS CR, Prague 2013*, pages 1–11, 2013.

[12] Kevin E.M. Church and Jean-Philippe Lessard. Codes for the work "Rigorous verification of Hopf bifurcations in functional differential equation"
`https://www.math.mcgill.ca/jplessard/ResearchProjects/HopfFDE/home.html`

[13] P.H. Coullet, C. Elphick, and E. Tirapegui. Normal form of a Hopf bifurcation with noise. *Physics Letters A*, 111(6):277–282, sep 1985.

[14] Jérôme Coville, Juan Dávila, and Salomé Martínez. Pulsating fronts for nonlocal dispersion and KPP nonlinearity. *Annales de l'Institut Henri Poincare (C) Analyse Non Lineaire*, 30(2):179–223, 2013.

[15] Michael G. Crandall and Paul H. Rabinowitz. The Hopf Bifurcation Theorem in infinite dimensions. *Archive for Rational Mechanics and Analysis*, 67(1):53–72, 1977.

[16] Carmen Da Silva and René Escalante. Segmented Tau approximation for a forwardbackward functional differential equation. *Computers & Mathematics with Applications*, 62(12):4582–4591, dec 2011.

[17] Babette de Wolff, Francesca Scarabel, Sjoerd Verduyn Lunel, and Odo Diekmann. Pseudospectral approximation of Hopf bifurcation for delay differential equations. pages 1–33, 2020.

[18] Annick Dhooge, Willy Govaerts, and Y. A. Kuznetsov. MATCONT: A MATLAB package for numerical bifurcation analysis of ODEs. *ACM Transactions on Mathematical Software*, 29(2):141–164, 2003.

[19] K. Engelborghs, T. Luzyanina, and D. Roose. Numerical bifurcation analysis of delay differential equations using DDE-BIFTOOL. *ACM Transactions on Mathematical Software*, 28(1):1–21, 2002.

[20] L. H. Erbe, W. Krawcewicz, K. Geba, and J. Wu. S1-degree and global Hopf bifurcation theory of functional differential equations. *Journal of Differential Equations*, 98(2):277–298, 1992.

[21] Neville J. Ford and Patricia M. Lumb. Mixed-type functional differential equations: A numerical approach. *Journal of Computational and Applied Mathematics*, 229(2):471–479, jul 2009.

[22] Neville J. Ford, Patricia M. Lumb, Pedro M. Lima, and M. Filomena Teodoro. The numerical solution of forwardbackward differential equations: Decomposition and related issues. *Journal of Computational and Applied Mathematics*, 234(9):2745–2756, sep 2010.

[23] S. Genieys, V. Volpert, and P. Auger. Pattern and waves for a model in population dynamics with nonlocal consumption of resources. *Mathematical Modelling of Natural Phenomena*, 1(1):63–80, 2006.

[24] Javier Gómez-Serrano. Computer-assisted proofs in PDE: a survey. *SeMA J.*, 76(3):459–484, 2019.

[25] Francois Hamel and Lenya Ryzhik. On the nonlocal Fisher-KPP equation: Steady states, spreading speed and global bounds. *Nonlinearity*, 27(11):2735–2753, 2014.

[26] Maoan Han and Weinian Zhang. On Hopf bifurcation in non-smooth planar systems. *Journal of Differential Equations*, 248(9):2399–2416, 2010.

[27] Jörg Härterich, Björn Sandstede, and Arnd Scheel. Exponential dichotomies for linear non-autonomous functional differential equations of mixed type. *Indiana University Mathematics Journal*, 51(5):1081–1109, 2002.

[28] Olivier Hénot. Polynomial embeddings of autonomous retarded functional differential equations. Preprint, 2020.

[29] H.J. Hupkes and S. M. Verduyn Lunel. Center manifold theory for functional differential equations of mixed type. *Journal of Dynamics and Differential Equations*, 19(2):497–560, 2006.

[30] Y. Kanzawa and S. Oishi. Calculating bifurcation points with guaranteed accuracy. *IEICE Trans. Fundamentals E82-A 6*, pages 1055–1061, 1999.

[31] I. Kmit and L. Recke. Hopf bifurcation for semilinear dissipative hyperbolic systems. *Journal of Differential Equations*, 257(1):264–309, 2014.

[32] Donald E. Knuth. *The art of computer programming. Vol. 2.* Addison-Wesley Publishing Co., Reading, Mass., second edition, 1981. Seminumerical algorithms, Addison-Wesley Series in Computer Science and Information Processing.

[33] Herbert Koch and Stuart S. Antman. Stability and Hopf bifurcation for fully nonlinear parabolic-hyperbolic equations. *SIAM Journal on Mathematical Analysis*, 32(2):360–384, 2000.

[34] Hans Koch, Alain Schenkel, and Peter Wittwer. Computer-assisted proofs in analysis and programming in logic: a case study. *SIAM Rev.*, 38(4):565–604, 1996.

[35] Hans Koch, Alain Schenkel, and Peter Wittwer. Computer-assisted proofs in analysis and programming in logic: a case study. *SIAM Rev.*, 38(4):565–604, 1996.

[36] Hiroshi Kokubu, Daniel Wilczak, and Piotr Zgliczyński. Rigorous verification of cocoon bifurcations in the Michelson system. *Nonlinearity*, 20(9):2147–2174, 2007.

[37] Yuri A Kuznetsov. *Elements of Applied Bifurcation Theory*, volume 112 of *Applied Mathematical Sciences*. Springer New York, New York, NY, 2004.

[38] Jean-Philippe Lessard. Rigorous verification of saddle-node bifurcations in ODEs. *Indag. Math. (N.S.)*, 27(4):1013–1026, 2016.

[39] J. P. Lessard and J. D. Mireles James. A functional analytic approach to validated numerics for eigenvalues of delay equations. *J. Comput. Dyn.*, 7(1):123–158, 2020.

[40] Jean-Philippe Lessard, J. D. Mireles James, and Julian Ransford. Automatic differentiation for Fourier series and the radii polynomial approach. *Phys. D*, 334:174–186, 2016.

[41] Jean-Philippe Lessard, Evelyn Sander, and Thomas Wanner. Rigorous continuation of bifurcation points in the diblock copolymer equation. *J. Comput. Dyn.*, 4(1-2):71–118, 2017.

[42] Zhihua Liu, Pierre Magal, and Shigui Ruan. Hopf bifurcation for non-densely defined Cauchy problems. *Zeitschrift fur Angewandte Mathematik und Physik*, 62(2):191–222, 2011.

[43] Shiwang Ma, Xiaoxin Liao, and Jianhong Wu. Traveling wave solutions for planar lattice differential systems with applications to neural networks. *Journal of Differential Equations*, 182(2):269–297, 2002.

[44] John Mallet-Paret and Sjoerd Verduyn Lunel. Exponential Dichotomies and Wiener-Hopf Factorizations for Mixed-Type Functional Differential Equations. *Journal of Differential Equations*, to appear, 2001.

[45] John Mallet-Paret and Sjoerd Verduyn Lunel. Mixed-Type Functional Differential Equations, Holomorphic Factorization, and Applications. *EQUADIFF 2003*, (February):73–89, 2003.

[46] Kaname Matsue. Rigorous verification of bifurcations of differential equations via the Conley index theory. *SIAM J. Appl. Dyn. Syst.*, 10(1):325–359, 2011.

[47] Teruya Minamoto and Mitsuhiro T. Nakao. Numerical method for verifying the existence and local uniqueness of a double turning point for a radially symmetric solution of the perturbed Gelfand equation. *J. Comput. Appl. Math.*, 202(2):177–185, 2007.

[48] B. P. Moghaddam, A. Dabiri, António M. Lopes, and J. A. Tenreiro Machado. Numerical solution of mixed-type fractional functional differential equations using modified Lucas polynomials. *Computational and Applied Mathematics*, 38(2):46, jun 2019.

[49] Grégoire Nadin, Benoît Perthame, and Min Tang. Can a traveling wave connect two unstable states? The case of the nonlocal Fisher equation. *Comptes Rendus Mathematique*, 349(9-10):553–557, 2011.

[50] Mitsuhiro T. Nakao, Michael Plum, and Yoshitaka Watanabe. *Numerical verification methods and computer-assisted proofs for partial differential equations*, volume 53 of *Springer Series in Computational Mathematics*. Springer, Singapore, 2019.

[51] Siegfried M. Rump. Verification methods: rigorous results using floating-point arithmetic. *Acta Numer.*, 19:287–449, 2010.

[52] Aldo Rustichini. Hopf bifurcation for functional differential equations of mixed type. *Journal of Dynamics and Differential Equations*, 1(2):145–177, apr 1989.

[53] Björn Sandstede and Arnd Scheel. Hopf Bifurcation From Viscous Shock Waves. *SIAM Journal on Mathematical Analysis*, 39(6):2033–2052, jan 2008.

[54] G. Schneider. Hopf Bifurcation in Spatially Extended Reaction-Diffusion Systems. *Journal of Nonlinear Science*, 8(1):17–41, 1998.

[55] D.J.W. Simpson and J.D. Meiss. Andronov-Hopf bifurcations in planar, piecewise-smooth, continuous flows. *Physics Letters A*, 371(3):213–220, nov 2007.

[56] Yongli Song, Junjie Wei, and Yuan Yuan. Bifurcation analysis on a survival red blood cells model. *Journal of Mathematical Analysis and Applications*, 316(2):459–471, 2006.

[57] R Szalai. Knut: A continuation and bifurcation software for delay-differential equations.

[58] Ken'ichiro Tanaka, Sunao Murashige, and Shin'ichi Oishi. On necessary and sufficient conditions for numerical verification of double turning points. *Numer. Math.*, 97(3):537–554, 2004.

[59] Filomena Teodoro, Pedro M. Lima, Neville J. Ford, and Patricia M. Lumb. New approach to the numerical solution of forward-backward equations. *Frontiers of Mathematics in China*, 4(1):155–168, mar 2009.

[60] Warwick Tucker. *Validated numerics*. Princeton University Press, Princeton, NJ, 2011. A short introduction to rigorous computations.

[61] Daniel Wilczak and Piotr Zgliczyński. Period doubling in the Rössler system—a computer assisted proof. *Found. Comput. Math.*, 9(5):611–649, 2009.

[62] Piotr Zgliczyński. Steady state bifurcations for the Kuramoto-Sivashinsky equation: a computer assisted proof. *J. Comput. Dyn.*, 2(1):95–142, 2015.